International Journal of Biological Macromolecules 346 (2026) 150678

Contents lists available at ScienceDirect

International Journal of Biological Macromolecules

journal homepage: www.elsevier.com/locate/ijbiomac

Microfluidic assembly and biomimetic lipid coating modulate the structure, stability, and biological interactions of P(DMAEMA-co-SMA)/DNA lipopolyplexes

Ioannis Tsichlis [a], Antiopi Vardaxi [b], Timothy Gomez [c], Antonia Athanasaki [d,e], Alexander Forys [f], Barbara Trzebicka [f], Simon C.W. Richardson [c], Kiriaki Chrissopoulou [d], Spiros H. Anastasiadis [d,e], Stergios Pispas [b], Dennis Douroumis [g], Costas Demetzos [a,*]

[a] Section of Pharmaceutical Technology, Department of Pharmacy, School of Health Sciences, National and Kapodistrian University of Athens, Panepistimioupolis Zografou, 15771, Athens, Greece
[b] Theoretical and Physical Chemistry Institute, National Hellenic Research Foundation, 48 Vassileos Constantinou Avenue, 11635, Athens, Greece
[c] Exogenics Laboratory, University of Greenwich at Medway, Faculty of Science and Engineering, Kent, ME4 4TB, UK
[d] Institute of Electronic Structure and Laser, Foundation for Research and Technology-Hellas, N. Plastira 100, 70013, Heraklion, Crete, Greece
[e] Department of Chemistry, University of Crete, Panepistimioupolis Vouton, 71003, Heraklion, Crete, Greece
[f] Centre of Polymer and Carbon Materials, Polish Academy of Sciences, 34 ul. M. Curie-Skłodowskiej, 41-819, Zabrze, Poland
[g] Department of Pharmacy, School of Life and Health Sciences, University of Nicosia, 29th Street, No. 17, Elliniko, 16777, Athens, Greece

ARTICLE INFO

Keywords:
DNA
Lipopolyplexes
Microfluidic assembly
pH-responsive cationic copolymer
Biomimetic lipid coating
Cytotoxicity
Cellular uptake

ABSTRACT

In this study, we present the development and characterization of biomimetic lipopolyplexes using the pH-responsive cationic copolymer, P(DMAEMA-co-SMA), DNA, and membrane-mimicking lipids. The copolymer was synthesized via RAFT polymerization and characterized by size exclusion chromatography, ^{1}H NMR spectroscopy, ATR-FTIR spectroscopy, and acid-base titration for proton buffering capacity. A custom-designed 3D-printed microfluidic chip with embedded microstructures was utilized to form polyplexes under controlled flow conditions, followed by a post lipid-coating step via lipid film hydration. The statistical copolymer P(DMAEMA-co-SMA) was utilized to condense DNA 50 bp at various nitrogen-to-phosphate (N/P) ratios, yielding polyplexes with distinct physicochemical characteristics. Lipid coating of preformed polyplexes enhanced colloidal stability under storage and biorelevant conditions, highlighting its critical role in maintaining nanoparticle integrity. Cryo-TEM analysis revealed the coexistence of multiple nanostructures with small-angle X-ray scattering (SAXS) supporting these findings and demonstrating pH-dependent organization that provides insights into their structural behavior under biologically relevant conditions. In vitro cytotoxicity and hemocompatibility assays indicated that the developed P(DMAEMA-co-SMA)/DNA lipopolyplexes are well tolerated compared to polyethylenimine (PEI), the gold standard in non-viral gene delivery. Confocal microscopy showed enhanced cellular uptake, endosomal escape, and cytoplasmic distribution in HeLa cells, supporting the potential of the prepared nanocomplexes for efficient intracellular gene delivery. Overall, this study presents P(DMAEMA-co-SMA)/DNA lipopolyplexes as a stable, biocompatible, and effective gene delivery platform and demonstrates how biomimetic lipid coating can modulate the stability and biological interactions of DNA nanocomplexes.

1. Introduction

In recent years, the delivery of genetic material, such as pDNA, mRNA, siRNA, and miRNA to cells has emerged as a promising approach for the treatment of severe disorders, including cancer, neurodegenerative diseases, and other genetic disorders (e.g., cystic fibrosis) [1]. Non-viral vectors, such as lipoplexes and polyplexes, offer several advantages in nucleic acid delivery, including low immunogenicity, high cargo capacity, and scale-up production. Despite their potential, lipoplexes often exhibit low transfection efficiency and cytotoxicity at high concentrations, while polyplexes face challenges such as limited stability [2]. To overcome these limitations, lipopolyplexes, hybrid complexes of

* Corresponding author.
E-mail address: demetzos@pharm.uoa.gr (C. Demetzos).

https://doi.org/10.1016/j.ijbiomac.2026.150678
Received 5 December 2025; Received in revised form 14 January 2026; Accepted 31 January 2026
Available online 2 February 2026

liposomes, polymers, and nucleic acids, have been developed as gene delivery vehicles that combine favorable properties of the above nanoplatforms, such as high stability, low cytotoxicity, efficient endosomal escape, and enhanced transfection efficiency [3,4].

Several studies demonstrate that lipopolyplexes, mainly composed of polyethylenimine (PEI) and cationic liposomes, enhance in vitro transfection efficiency, improve colloidal stability, and retain physicochemical integrity during prolonged storage compared to polyplexes [5,6]. However, PEI is associated with significant cytotoxicity even at low concentrations and lacks biodegradability, resulting in potential accumulation following in vivo administration [7]. In this context, limited research has been conducted on lipopolyplexes consisting of poly(2-(dimethylamino)ethyl methacrylate) (PDMAEMA), despite its potential as a promising alternative to PEI, with lower cytotoxicity, and transfection efficiency approximately 90% of branched PEI (25 kDa) [8].

Lipid coating of polyplexes has emerged as a promising strategy to combine the advantages of cationic polymers and lipids within a single core-shell nanostructure. Lipopolyplexes, in which a nucleic acid-polycation core is surrounded by a lipid layer, have been shown to improve colloidal stability, reduce cytotoxicity, and enhance transfection efficiency compared to lipoplexes and polyplexes [9–13]. Notably, cationic lipid-coated PEI/DNA polyplexes and other PEI-based lipopolyplexes have displayed higher serum stability and more efficient gene delivery, while mitigating PEI-associated cytotoxicity. Therefore, lipid-polymer hybrid nanoparticles provide a versatile platform in which the lipid composition and polymer structure can be modified to control nanoparticle properties, encapsulation efficiency, and biological interactions. These studies highlight the potential of lipid-coated polymer-nucleic acid complexes as next-generation non-viral gene delivery systems and highlight the critical influence of lipid composition and macromolecular organization on their structure, stability, and biological behavior.

PDMAEMA is a cationic polyelectrolyte with tertiary amino groups that exhibits pH- and thermo-responsive properties, making it suitable for nucleic acid condensation. With a pKa of approximately 7.4, PDMAEMA remains partially protonated under physiological conditions, and, thus, positively charged, facilitating electrostatic interactions with negatively charged biomolecules such as nucleic acids [14,15]. At pH 4, PDMAEMA is fully protonated, water-soluble, and its thermo-responsive behavior is eliminated. In contrast, at pH 7.4, PDMAEMA exhibits a thermal transition with a Lower Critical Solution Temperature (LCST) of approximately 45 °C, which depends mainly on its molar mass [16]. The molar mass of PDMAEMA plays a crucial role in gene delivery, as polymers with high molar mass form smaller polyplexes and enhance transfection efficiency, although with increased cytotoxicity [8].

Hydrophobic modification of cationic polymers has been reported as an effective strategy to enhance nucleic acid condensation through cooperative hydrophobic interactions in addition to electrostatic complexation. These interactions can promote the formation of more compact polyplexes, improving colloidal stability and cellular uptake. Amphiphilic copolymers containing long alkyl methacrylate side chains have been shown to self-assemble with nucleic acids into more compact and colloidally stable nanocomplexes compared to purely hydrophilic polycations, while also exhibiting reduced cytotoxicity [17,18]. In this context, the incorporation of hydrophobic methacrylate units into PDMAEMA-based copolymers imparts amphiphilic character to the copolymer, which can promote polyplex assembly and biological interactions [19–21]. Accordingly, the stearyl methacrylate (SMA) segments in the synthesized P(DMAEMA-*co*-SMA) statistical copolymer are expected to support polyplex formation through hydrophobic association and facilitate subsequent lipid coating, leading to the formation of stable lipid-polymer hybrid nucleic acid assemblies for efficient gene delivery.

Conventional methods for polyplex formation, such as standard pipetting, often result in physicochemical heterogeneous dispersions, batch-to-batch variability, and limited control over nanoparticle size. Moreover, the sequence of polyelectrolyte addition affects the physicochemical properties of the resulting polyplexes, including size, size distribution, and stability [22,23]. In contrast, microfluidic development enables precise control of the self-assembly process, resulting in reproducible and more uniform gene delivery nanoplatforms. This approach is favorable for nanoparticle formation and allows fine-tuning of nanoparticle properties (i.e., size, polydispersity index) by adjusting critical parameters, including flow rates and chip geometry [24,25].

The aim of the present study was to develop and characterize P(DMAEMA-co-SMA)/DNA polyplexes using DNA 50 bp as a model biological macromolecule, and to investigate how biomimetic lipid coating influences their structure, colloidal stability, and biological interactions. Polyplexes were prepared by both conventional mixing and a custom 3D-printed microfluidic chip, with lipid coating applied to the microfluidic-assembled polyplexes to form lipopolyplexes. The resulting nanocomplexes were characterized physicochemically, analyzed morphologically and structurally using cryo-TEM and SAXS, and assessed in vitro for cytotoxicity, hemocompatibility and cellular uptake. This study highlights the potential of P(DMAEMA-co-SMA) for nucleic acid condensation and demonstrates the critical role of microfluidic assembly followed by biomimetic lipid coating in enhancing colloidal stability and maintaining overall integrity for effective intracellular gene delivery.

2. Materials and methods

2.1. Materials

The lipids 1,2-distearoyl-sn-glycero-3-phosphocholine (DSPC), 1,2-dioleoyl-sn-glycero-3-phosphoethanolamine (DOPE), 1,2-dioleoyl-3-trimethylammonium-propane (chloride salt) (DOTAP), cholesterol, and sphingomyelin (Egg, Chicken) (SM) were generously provided by Lipoid (GmbH, Ludwigshafen, Germany) and used without further purification. The amphiphilic copolymer P(DMAEMA-co-SMA) was synthesized as described with an average molecular mass of 53,900 g/mol. PEI 50 kDa and DNA 50 bp from herring sperm (hsDNA) were obtained from Sigma-Aldrich Chemical Co (St. Louis, MO, USA). Chloroform and ethanol were of analytical grade and acquired from Sigma-Aldrich Chemical Co (St. Louis, MO, USA). Phosphate Buffered Saline (PBS) tablets, sodium citrate, and citric acid salts were obtained from Sigma-Aldrich Chemical Co (St. Louis, MO, USA) and dissolved in HPLC grade water (Thermo Fischer Scientific Inc., Germany) at appropriate concentrations.

2.2. 3D printing of microfluidic chip

The microfluidic device was designed using CAD software (SolidWorks, Dassault Systèmes) with two threaded inlet ports (8 mm length, 28 threads per inch) connected to independent rectangular channels (500 μm width, 300 μm height). These channels merge into a serpentine mixing channel (765 μm width, 300 μm height, 3.5 cm length) connected to a single outlet. Fin-like structures (153 μm length, 68 μm width, and 85.1 μm spacing between fins) with repeated patterns were integrated within the mixing channel over 32 cycles.

The microfluidic chip was fabricated using a digital light processing (DLP) 3D printer (Asiga MAX X27, Asiga, Germany), equipped with a 385 nm ultraviolet (UV) DLP projector and a 27 μm pixel size. A low-viscosity microfluidic resin was used as the printing material. The designs, initially saved in .prt format, were converted into .stl files compatible with the printer's slicing software (Composer 2.1, Asiga). The chip structure was oriented flat on the build plate for slicing, with no additional support required. The slicing parameters included a layer thickness of 25 μm, UV intensity of 3 mW/cm^2, and an exposure time of 3.3 s per layer. For the initial layer, the exposure time was extended to 112 s to ensure proper adhesion to the build plate.

After fabrication, the microfluidic chip was detached from the build plate and immersed in isopropanol for 10 min to remove residual

uncured resin from the surface. Internal channels were flushed with isopropanol over five cycles to eliminate residual resin. The chip was then air-dried for a minimum of 4 h. To complete polymerization and optimize the mechanical and chemical properties of the structure, the chip was cured in a UV-A heated chamber (MeccatroniCore BB Cure Dentalstation, GoPrint3D, Ripon, North Yorkshire, UK) at 40 °C for 60 min [26].

2.3. Scanning electron microscopy (SEM) analysis of the microfluidic chip

Scanning Electron Microscopy (SEM) was used to evaluate the printing accuracy of Digital Light Processing (DLP) technology in fabricating microfluidic devices for nanoparticle preparation. Open microfluidic designs with identical structural details to their closed-array counterparts were 3D-printed using the same DLP technique. SEM imaging was performed using a Hitachi SU8030 system (Tokyo, Japan), operated at an electron beam accelerating voltage of 1.0 kV and a magnification of 30×, to capture detailed surface morphology and structural integrity.

2.4. Synthesis of P(DMAEMA-co-SMA) copolymer

P(DMAEMA-*co*-SMA) statistical copolymer was synthesized via one-step reversible addition-fragmentation chain transfer (RAFT) polymerization. First, a column containing monomethyl ether hydroquinone (MEHQ) and butylated hydroxytoluene (BHT) inhibitor removers was used to purify DMAEMA and SMA monomers. In a round bottom flask (25 mL), purified DMAEMA (0.8 g, 5.09 mmol) and SMA (0.2 g, 5.91 mmol) were mixed with CDP (0.081 g, 0.2 mmol), AIBN (0.0033 g, 0.02 mmol) (at CDP: AIBN = 10:1 ratio) and 0.575 mL 1,4-dioxane (20 wt% monomer solution) while being stirred magnetically. The flask was sealed with a rubber septum, and the solution was degassed using a nitrogen gas flow for 20 min. The flask was then submerged in a pre-heated oil bath at 70 °C for 24 h under magnetic stirring. The reaction was quenched by freezing at −20 °C for 30 min followed by exposure to air. The reaction product was purified by dialysis against deionized water using 3.5 kDa MWCO dialysis membranes to remove unreacted monomers and impurities. The outer water reservoir was periodically changed over the three days of purification. The pure copolymer was isolated using a rotary evaporator and dried in a vacuum oven at 25 °C for 24 h [15].

2.5. Size-exclusion chromatography

The weight average molecular mass (M_w) and molecular mass distribution (M_w/M_n) of P(DMAEMA-co-SMA) statistical copolymer were determined by size exclusion chromatography (SEC) using a Waters system (Waters Corporation, Milford, MA, USA). The setup included a Waters 1515 isocratic pump, three μ-Styragel mixed pore separation columns (pore size 102–106 Å), and a Waters 2414 refractive index detector equilibrated at 40 °C. THF with 5% *v*/v triethylamine was used as the eluent at a flow rate of 1 mL/min at 30 °C. Data analysis was performed using Breeze software (version 3.2). The chromatographic instrument was calibrated using standard polystyrene samples with narrow molecular weight distributions and average molecular weights ranging from 1200 to 929,000 g/mol [15].

2.6. Proton nuclear resonance (^1H NMR) spectroscopy

^1H NMR spectroscopy was utilized to determine the chemical structure and mass composition (%wt) of P(DMAEMA-co-SMA) copolymer. Spectrum was collected using a Varian 300,600 MHz spectrometer (California) with tetramethylsilane (TMS) as the internal standard in deuterated chloroform. For sample preparation, 10 mg of dry copolymer were dissolved in 700 μL of deuterated chloroform.

2.7. Attenuated total reflectance-Fourier transform infrared spectroscopy (ATR-FTIR)

ATR-FTIR spectroscopy was performed to qualitatively confirm the molecular characteristics of the copolymer. Bruker Optik Fourier transform instrument (Germany), equipped with a press and an attenuated total reflectance diamond accessory (Dura-Samp1IR II by SensIR Technologies, Chapel Hill, NC, USA), was used to collect the FTIR spectrum. The copolymer was measured in dry state at room temperature.

2.8. Determination of proton buffering capacity

The proton buffering capacity of P(DMAEMA-co-SMA) was determined using the acid-base titration method [27]. Briefly, 6 mg of P(DMAEMA-co-SMA) was dissolved in 30 mL of NaCl solution (150 mM), and the pH of the solution was adjusted to 10 using NaOH (0.1 M). PEI and NaCl were used as positive and negative controls, respectively. Aliquots of HCl (0.1 M, 50 μL) were added to the solutions, which were titrated until pH 3.5 using a pH meter (Mettler Toledo, Greifensee, Switzerland) [28]. The proton buffering capacity was calculated for the pH range of 7.4–5.1 according to Eq. (1) and is expressed as mmol H^+ per unit pH change:

$$\text{Buffer capacity } (\beta) = \frac{\Delta HCl_{mol}}{\Delta pH} \quad (1)$$

2.9. Development of polyplexes by standard pipetting method

For the formation of P(DMAEAMA-co-SMA)/DNA polyplexes, a standard stock solution of the copolymer (1 mg/mL) in citrate buffer (20 mM, pH 4) was used. DNA solutions in citrate buffer were also prepared, according to the intended copolymer nitrogen to DNA phosphate (N/P) ratio. Complexation was achieved at N/P ratios ranging from 4 to 14, by adding the appropriate DNA solution dropwise into a constant volume of the copolymer solution, under gentle stirring at room temperature [21]. The formed polyplexes were incubated at room temperature for physicochemical analysis.

2.10. Microfluidic development of polyplexes

P(DMAEAMA-co-SMA)/DNA polyplexes were formed at the same N/P ratios using the 3D-printed microfluidic chip connected to a dual-channel syringe pump (IPS independent 14R, Inovenso Ltd. Co., Turkey). One syringe was loaded with a copolymer solution, and the other one with a DNA solution. The concentrations of the solutions were determined based on the positive charges of the DMAEMA amino groups (N) and the negative charges of the DNA phosphate groups (P) [29]. The copolymer and DNA solutions were pumped into the chip at a 4:1 (*v*/v) flow rate ratio, with a total flow rate of 1 mL/min. The resulting polyplexes were incubated at room temperature for physicochemical characterization.

2.11. Development of lipopolyplexes

P(DMAEMA-co-SMA)/DNA lipopolyplexes were prepared by a two-step process, in which the first step included the condensation of the DNA with the copolymer in citrate buffer (20 mM, pH 4) to form polyplexes, and followed by lipid coating using the thin film hydration method/extrusion, as described in the literature, with a final lipid concentration of 10 mg/mL [30]. Specifically, lipids (DSPC, DOPE, DOTAP, cholesterol, sphingomyelin) were dissolved in chloroform (10 mg/mL) and aliquots of the stock solutions were mixed into a round-bottom flask to achieve the desired molar ratio (DSPC:DOPE:DOTAP:Chol:SM 45:35:3:10:7). The solvent was evaporated under vacuum at 40 °C for 30 min using a rotary evaporator, and a thin lipid film was developed.

Pre-formed P(DMAEMA-co-SMA)/DNA polyplexes prepared via microfluidics at N/P 4, were used to hydrate the lipid film by gentle stirring in a water bath for 1 h, resulting in a final lipid concentration of 10 mg/mL. The dispersion was extruded 10 times through polycarbonate membranes of 400 nm pore size using a liposome extruder to reduce particle size and achieve homogenization. The resulting lipopolyplexes were dialyzed overnight against phosphate buffered saline (PBS, pH 7.4) using a Spectra-Por® Float-A-Lyzer® (MWCO 20 kDa, Spectrum Labs, Rancho Dominguez, CA) to neutralize the external pH while retaining the unbound DNA for the encapsulation efficiency determination. For all further experiments, the unencapsulated DNA was removed by dialysis using a Spectra-Por® Float-A-Lyzer® with a 50 kDa MWCO [31].

2.12. Stability of lipopolyplexes upon storage

The storage stability of P(DMAEMA-co-SMA)/DNA lipopolyplexes was studied at 4 °C by measuring physicochemical characteristics at predetermined time points for up to 84 days. Specifically, the hydrodynamic diameter (D_h) and size distribution (polydispersity index, PDI), were assessed using dynamic light scattering (DLS). The ζ-potential of the nanoparticles was determined by electrophoretic light scattering (ELS). Measurements were conducted at 25 °C (detection angle 90°) with a photon correlation spectrometer (Zetasizer ZSU3105, Malvern, UK) and analysis was performed by the ZS XPLORER software (Malvern software). For the measurements, 50 μL of each sample was diluted 20-fold in HPLC grade water [32,33].

2.13. Colloidal stability of lipopolyplexes in biorelevant conditions

The colloidal stability of P(DMAEMA-co-SMA)/DNA lipopolyplexes was assessed under simulated intracellular pH conditions by diluting samples 20-fold in citrate buffer solutions at pH 6.5, 5.5, and 4.5, corresponding to the environment of early endosomes, late endosomes, and lysosomes, respectively. The diluted samples were incubated at 37 °C for 30 min and analyzed using DLS under the same conditions described above [34]. The physicochemical properties of lipopolyplexes were also monitored after incubation in complete cell culture medium (DMEM supplemented with 10% fetal bovine serum 2 mM glutamine, penicillin and streptomycin) at 37 °C using DLS. For the measurements, 50 μL of the sample was diluted 20-fold in complete medium. Measurements were performed at predetermined time points (0, 1 h, 2 h, 3 h, 4 h, 5 h, 6 h, 24 h) to evaluate the colloidal stability of the nanoparticles under cell culture conditions [35,36].

2.14. Encapsulation efficiency (EE%) determination

The encapsulation efficiency (EE%) of DNA was determined using Qubit™ 1× dsDNA High Sensitivity Kit (Thermo Fisher Scientific, Waltham, Massachusetts, USA). For the quantification of the non-encapsulated DNA, lipopolyplexes were diluted in TE buffer along with the dsDNA reagent. For the quantification of the total amount of DNA, lipopolyplexes were treated with 1% Triton X-100 and incubated for 5 min, followed by dilution in TE buffer and dsDNA reagent [31,37]. DNA concentrations were measured using a Qubit™ 4 Fluorometer device (Thermo Fisher Scientific, Waltham, Massachusetts, USA) following the manufacturer's instructions. A standard curve was generated using the supplied DNA standards, and the encapsulation efficiency (EE)% was calculated using the following equation:

$$(EE)\% = \left(1 - \frac{C_{free\ DNA}}{C_{total\ DNA}}\right) \times 100 \quad (2)$$

2.15. Cryogenic transmission electron microscopy (Cryo-TEM)

Cryogenic transmission electron microscopy (Cryo-TEM) images were obtained using a Tecnai F20 X TWIN microscope (FEI Company, USA) equipped with a field emission gun, operating at an accelerating voltage of 200 kV. The images were recorded on a Gatan Rio 16 CMOS 4k camera (Gatan Inc., USA) and processed with Gatan Microscopy Suite (GMS) software (version 3.31.2360.0). Specimen preparation involved vitrification of the aqueous dispersion on grids with holey carbon film (Quantifoil R 2/2; Quantifoil Micro Tools GmbH, Germany). The grids were pre-activated for 15 s in oxygen plasma using a Femto plasma cleaner (Diener Electronic, Germany). Cryo-samples were prepared by applying a droplet (3 μL) of the dispersion (1 mg/mL) to the grid, blotting with filter paper, and immediately freezing in liquid ethane using a fully automated blotting device, Vitrobot Mark IV (FEI Company, USA). After preparation, the vitrified specimens were kept under liquid nitrogen until they were inserted into a cryo-TEM holder Gatan 626 (Gatan Inc., USA) and analyzed in the TEM at −178 °C [38].

2.16. Small-angle X-ray scattering (SAXS)

The SAXS measurements of the developed P(DMAEMA-co-SMA)/DNA lipopolyplexes at a concentration of 1 mg/mL were performed at pH 7.4, 5.5 and 4.5 to evaluate the structural organization under formulation and under biorelevant conditions mimicking endosomal and lysosomal environments, respectively. Measurements were carried out using a Xeuss 3.0 laboratory system (Xenocs, France), equipped with a Xenocs low-noise flow cell operating under dynamic vacuum. The X-ray beam had an energy of 8 keV (λ = 1.54 Å). The wavevector (q)-scale was calibrated using scattering profiles from silver behenate (AgBeh) and lanthanum hexaboride (LaB_6). Measurements were collected with a high-resolution collimation setup, employing a 2D photon-counting hybrid detector (Eiger2 R 1 M) at a sample-to-detector distance set to 500 mm and an acquisition time of 40 min.

2.17. Cell culture and cell proliferation assay

Human cervical cancer cells (HeLa; ATCC® CCL-2, RRID: CVCL_0030) were cultured (1×10^4 cells/well) into a 96-well plate in DMEM supplemented with 10% (*v*/v) Fetal Bovine Serum (FBS) and 2 mM glutamine, as well as penicillin and streptomycin (Gibco-Life Technologies, Grand Island, NY, USA). The cells were cultured in a CO_2 incubator at 37 °C with 90% humidity and 5% (v/v) CO_2. The MTT assay was used to determine cell viability. Cells were incubated with empty lipid-polymer hybrid nanoparticles and lipopolyplexes for 24 h, at a wide range of total formulation concentrations (1–400 μg/mL). PEI and dextran were used as positive and negative controls, respectively. An additional MTT assay was conducted after 72 h incubation with lipopolyplexes over the same concentration range. Following treatment, the mitochondrial redox function expressed as cell viability was assessed by the MTT assay (Sigma-Aldrich, St. Louis, MO, USA). The cell medium in each well was replaced with MTT solution (1 mg/mL in complete media), and cells were incubated at 37 °C for 4 h. Subsequently, the MTT was removed from all cells, and the produced formazan crystals were solubilized with DMSO. The plates were shaken briefly, and the absorbance was measured at 560 nm. Cell viability was calculated in comparison to untreated cells, which served as controls.

2.18. Hemolysis assay

The hemolytic activity of the prepared P(DMAEMA-co-SMA)/DNA lipopolyplexes was evaluated. Specifically, blood was collected from mice into heparinized tubes and centrifuged at 2000 ×*g* for 10 min. The resulting red blood cell (RBC) pellet was washed three times with phosphate-buffered saline (PBS, pH 7.4), each time centrifuging at 2000 ×*g* for 10 min. The final RBC suspension was prepared in PBS (2%, *w*/*v*) and used within 24 h of collection. Samples were prepared at various concentrations in PBS and incubated with an equal volume of the RBC suspension for 30 min at 37 °C. PEI was used as a positive control. After incubation, samples were centrifuged at 2000 ×*g* for 10 min, and the

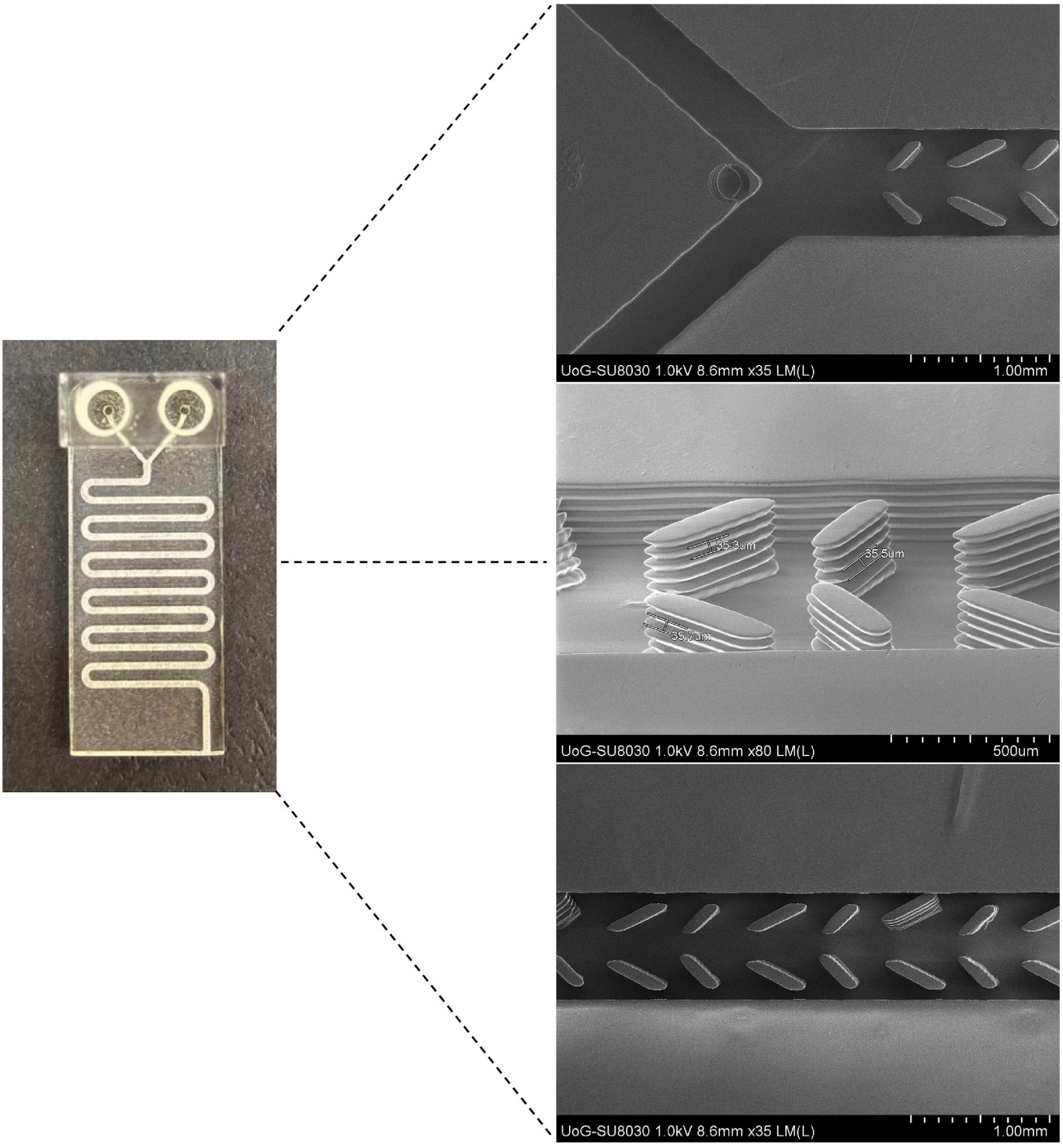

Fig. 1. SEM images of the 3D-printed serpentine microfluidic chip.

absorbance of the supernatant (100 μL) was measured at 540 nm using a UV–Vis spectrophotometer to quantify hemoglobin release. The results were expressed as the percentage of hemoglobin released compared to the release induced by 1% Triton X-100 (100% control) [39].

2.19. Confocal laser scanning microscopy (CLSM)

Imaging was performed using an LSM880 with Airyscan unit from Carl Zeiss. For cellular uptake study, HeLa cell images were acquired after seeding HeLa cells (ECCAC 93021013) at a density of 1×10^5 cells/well in 35 mm dishes containing a sterile coverslip each. Prior to fixation (24 h) the lipopolyplex was added to serum-free media bathing the cells, which were incubated under standard conditions. Cells were fixed in 2% (*w/v*) formalin in PBS and mounted in 1% (w/v) N-propyl gallate contained in PBS and sealed using nail varnish after staining with DAPI (100 nm) and Alexafluor-488-labelled phalloidin, following the manufacturer's instructions. Cells were imaged using the Alexafluor-488 channel and separately the Texas Red channel and were exported as TIFF files. For the intracellular distribution of lipopolyplexes, Hela cells were seeded at a density of 1×10^5 cells/well in 35 mm dishes

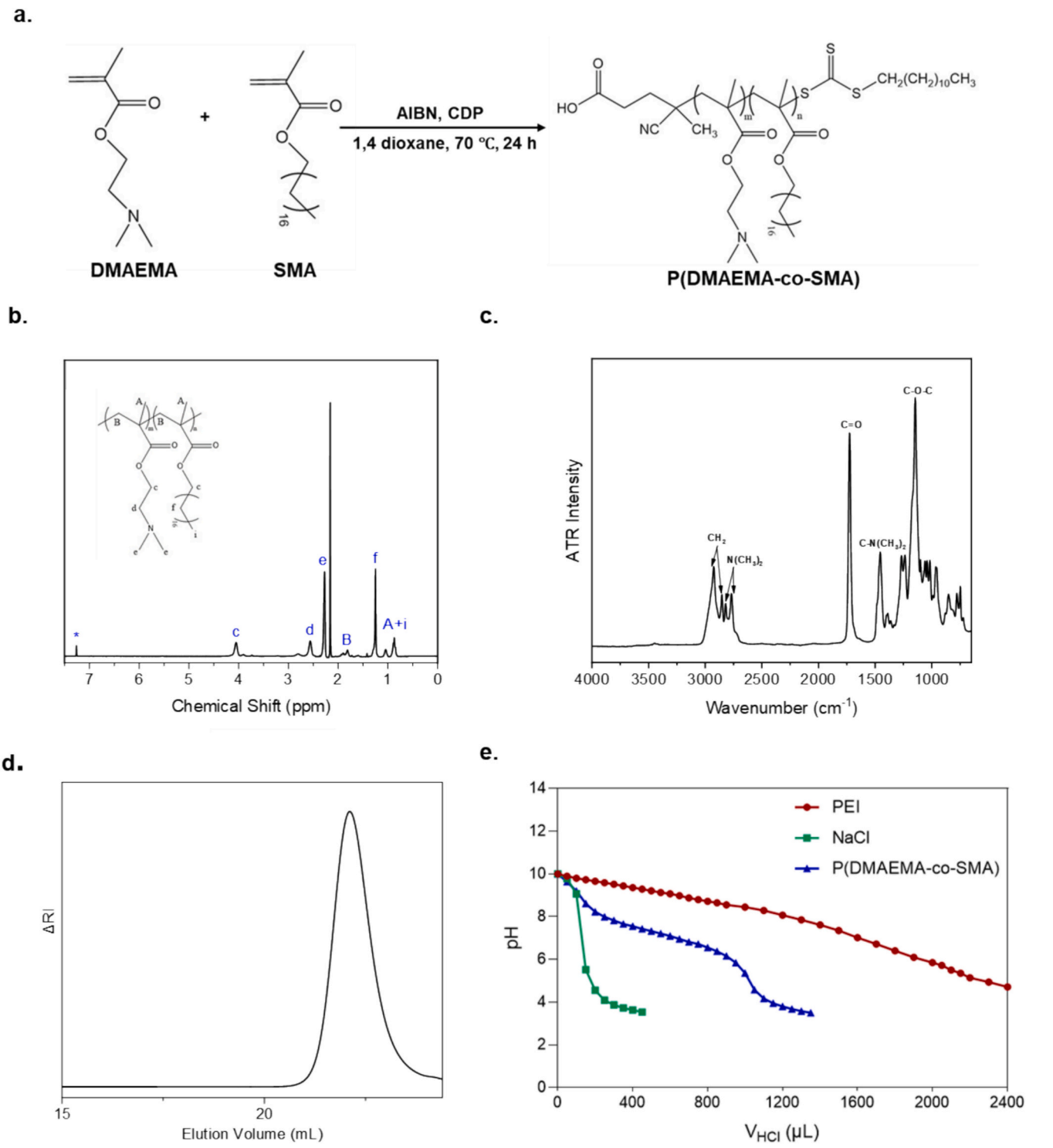

Fig. 2. (a) Synthesis of the statistical copolymer P(DMAEMA-*co*-SMA) via RAFT polymerization. Characterization of the copolymer by (b) ^{1}H NMR spectroscopy in deuterated chloroform (signal denoted by an asterisk in the spectrum), (c) ATR-FTIR spectroscopy, (d) size-exclusion chromatography (SEC), and (e) acid-base titration for buffering capacity.

containing a sterile coverslip each. The following day, they were incubated with the rhodamine-labelled lipopolyplexes at 50 μg/mL and left for 24 h under standard incubation conditions. After 20 h of incubation with the lipopolyplexes, 5 μg/mL wheatgerm agglutinin labelled with Alexafluor-488 was added to the cells. After this time, the cells were fixed as before, mounted and imaged. Cells were imaged using the Alexafluor-488 channel and separately the Texas Red channel.

2.20. Statistical analysis

The statistical analysis was performed using GraphPad Prism 8.0 software package (San Diego, USA). All experiments were performed in triplicate. Results are reported as the mean ± standard deviation. Statistical significance was evaluated using one-way ANOVA followed by Tukey's post hoc test. Physicochemical properties of polyplexes prepared by standard pipetting and microfluidics, as well as in vitro cytotoxicity

data were analyzed using two-way ANOVA followed by Bonferroni post-hoc test. A p-value < 0.05 was considered statistically significant.

3. Results and discussion

3.1. Design of the 3D-printed microfluidic chip

Microfluidic development of nanoparticles has gained significant attention in recent years, particularly for polyplexes formed through electrostatic interactions, where precise control over nanoparticle size and size distribution remains challenging. Microfluidic mixing occurs at the micrometer scale under low Reynolds numbers ($Re < 2000$), where laminar flow provides a more predictable and controllable mixing compared to turbulent flow, although with limited mixing efficiency [40]. Enhanced mixing efficiency can result in smaller and more uniform nanoparticles [41]. Therefore, microfluidic devices with embedded microstructures have been developed to disrupt laminar flow and induce chaotic advection, thus enhancing mixing efficiency [42]. In this study, we present a novel serpentine microfluidic chip with embedded fin-like microstructures, fabricated using Digital Light Processing (DLP) 3D printing technology (Fig. 1). Serpentine microchannels enhance mixing through Dean vortices, which are secondary flows induced by curved regions. In our design, this effect is extended to the straight segments by incorporating microstructures specifically engineered to disrupt laminar flow and promote chaotic advection. As a result, mixing efficiency is enhanced throughout the entire channel. This hybrid design enables continuous, efficient, and spatially uniform mixing between two fluids compared to conventional serpentine microfluidic devices, offering an advanced platform for the controlled synthesis of nanoparticles.

DLP 3D printing was selected for its capability to produce complex geometries with high resolution (Fig. S1). This technology enables precise adjustments to the geometry and dimensions of the microstructures, including height, width, and length, while maintaining high fabrication quality. SEM images highlight the precise fabrication and structural integrity of the microfluidic chip, confirming that DLP is an effective technology for designing microfluidic devices with embedded, customizable microstructures. The serpentine channel and fin-like microstructures are well-defined, with fin dimensions of 153 μm in length, 68 μm in width, and 85.1 μm spacing between fins. Each fin has a thickness of 35.5 μm, demonstrating precise fabrication process. The consistent reproduction of the microstructures highlights the accuracy and high resolution achieved through DLP 3D printing. The channel width of 765 μm provides sufficient space for fluid flow while maintaining a design optimized for efficient mixing.

3.2. Synthesis and characterization of P(DMAEMA-co-SMA) copolymer

The statistical copolymer poly(2-(dimethyl amino ethyl methacrylate)-*co*-(stearyl methacrylate)), P(DMAEMA-*co*-SMA) was synthesized via RAFT polymerization using a one-step synthesis procedure. Its structural and molecular characteristics were studied using ^{1}H NMR spectroscopy, ATR-FTIR spectroscopy, size-exclusion chromatography, and buffering capacity (Fig. 2).

RAFT polymerization was performed instead of ATRP (atom transfer radical polymerization) to avoid toxic organometallic catalysts and obtain a low dispersity (Đ) indicative of narrow molecular mass distribution. The copolymer was designed with a specific molar mass and composition, incorporating the SMA segments, as hydrophobic monomers have been widely used to enhance transfection efficiency and reduce the cytotoxicity of PDMAEMA [43]. 4-Cyano-4-(dodecylsulfanylthiocarbonyl)pentanoic acid (CDP) was utilized as the chain transfer agent for the synthesis of the copolymer, as it is suitable for methacrylate-based monomers. The molecular characterization of the copolymer by size-exclusion chromatography (SEC) revealed a molar mass close to the theoretical stoichiometry, and a dispersity (M_w/M_n) within the typical range reported for statistical copolymers synthesized via RAFT polymerization (Table 1).

Table 1
Molecular characteristics of P(DMAEMA-co-SMA) copolymer.

Statistical copolymer	Mw ($g*mol^{-1}$) ($\times 10^4$) (SEC)	Mw/Mn (SEC)	%wt. DMAEMA (^{1}H NMR)	%wt. SMA (^{1}H NMR)
P(DMAEMA-co-SMA)	5.39	1.16	79	21

The chemical structure and composition of the synthesized copolymer were determined using ^{1}H NMR spectroscopy in deuterated chloroform ($CDCl_3$). The residual proton signal of chloroform ($CHCl_3$) present in the deuterated solvent is indicated by an asterisk (*) at 7.2 ppm. The sharp singlet observed at approximately 2.2 ppm is attributed to trace residual acetone rather than to the copolymer structure. This signal is well separated from the polymer resonances, and the chemical compositions can be effectively evaluated. Specifically, characteristic peaks corresponding to DMAEMA (2.3 ppm) and SMA (1.25 ppm) monomers were identified in the ^{1}H NMR spectrum (Fig. 2b) [15,44]. The chemical composition of each monomer in the statistical P(DMAEMA-co-SMA) copolymer was estimated by analyzing the integrals of the characteristic peaks. ATR-FTIR spectroscopy (Fig. 2c) confirms the chemical composition of the copolymer, obtained by ^{1}H NMR. Moreover, the chromatogram of P(DMAEMA-co-SMA) demonstrated efficient purification from unreacted SMA monomers via dialysis against deionized H_2O. The copolymer exhibited a monomodal and relatively narrow peak with minimal tailing, which indicates a well-controlled polymerization process (Fig. 2d). The proton buffering capacity of P(DMAEMA-co-SMA) was determined using the acid-base titration method within the pH range of 7.4–5.1, as it directly affects endosomal escape prior to lysosomal degradation by nucleases [45]. In general, a high amount of protons required to shift the solution pH indicates that the polymer has a strong tendency to be protonated, and, consequently, a strong buffering capacity [46]. The results indicate that the copolymer exhibits a lower buffering capacity (0.024 mmol H^+ per unit pH change) compared to PEI (0.033 mmol H^+ per unit pH change) within the pH range of 7.4–5.1, as shown in Fig. 2e. This finding can be attributed to the reduced number of amine groups of PDMAEMA compared to PEI, although the sterically unhindered tertiary amines of PDMAEMA exhibit a higher intrinsic capacity to absorb protons [28,47]. Despite the lower buffering capacity, the copolymer appears to retain sufficient potential for endosomal escape. Previous studies indicate that the proton sponge effect in PDMAEMA and its derivatives is less pronounced compared to PEI, however, alternative mechanisms, such as membrane destabilization, maintain the polymer's capacity for endosomal escape [48–50].

3.3. P(DMAEMA-co-SMA)/DNA polyplexes prepared via conventional pipetting versus microfluidics

The development of polyplexes for gene delivery presents a significant challenge in the precise control of physicochemical properties, which is essential for enhancing cellular uptake and minimizing cytotoxicity. P(DMAEMA-co-SMA), a cationic amphiphilic statistical copolymer with a tertiary amine group, was used to enhance electrostatic interactions with the negatively charged DNA at pH 4, where the copolymer is fully protonated. P(DMAEMA-co-SMA)/DNA polyplexes at various copolymer nitrogen to DNA phosphate (N/P) ratios were prepared using both conventional pipetting and microfluidics. For microfluidic preparation, DNA and copolymer solutions were pumped into the fabricated 3D-printed microfluidic chip under controlled flow conditions, with a total flow rate (TFR) of 1 mL/min and a flow rate ratio (FRR) of 4:1. The hydrodynamic diameter (D_h), polydispersity index (PDI), and aggregation behavior were studied.

Regarding the hydrodynamic diameter (Fig. 3), microfluidic

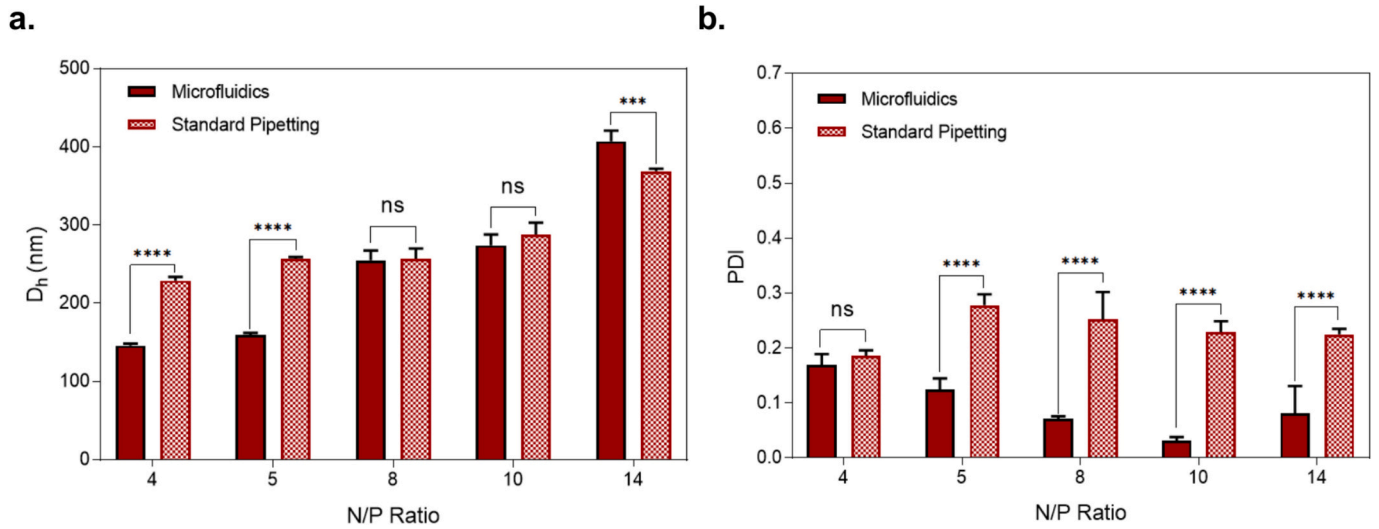

Fig. 3. (a) The hydrodynamic diameter and (b) polydispersity index of P(DMAEMA-*co*-SMA)/DNA polyplexes prepared by conventional pipetting and microfluidics at different N/P ratios. Statistical analysis was performed using two-way ANOVA followed by Bonferroni post hoc test. Significant differences between preparation methods are denoted (****$p < 0.0001$; ***$p < 0.001$; ns, no significance).

development resulted in smaller polyplexes compared to conventional pipetting at N/P ratios ranging from 4 to 10. However, microfluidic polyplexes formed at N/P 14 exhibited larger size compared to conventional pipetting. Specifically, at N/P 4, microfluidic polyplexes exhibited a hydrodynamic diameter nearly 50% smaller than those prepared by the conventional method, a statistically significant result that persisted at N/P 5 ($p < 0.0001$). This result can be attributed to the precise and rapid mixing dynamics of the microfluidic chip, which facilitates efficient DNA complexation and condensation. In contrast, standard pipetting depends on manual mixing, thus leading to larger and more heterogeneous polyplexes [22]. According to Liu et al., variations in size are crucial, as smaller polyplexes are associated with higher transfection efficiency and lower cytotoxicity [51]. Nevertheless, a specific trend was observed in the hydrodynamic diameter of polyplexes as a function of N/P ratio for both preparation methods. Specifically, increasing the N/P ratio, and consequently the number of available positive charges from the amino group, resulted in higher D_h values. This indicates the formation of larger polyplexes with higher molar mass and a tendency to form aggregates [21].

As shown in Fig. 3, the PDI of microfluidic polyplexes was consistently lower compared to polyplexes prepared by standard pipetting, indicating a more uniform size distribution. Both methods resulted in comparable PDI values at N/P 4, however, significant differences were observed at higher N/P ratios. The greatest variation was observed between N/P 5 and 14, where microfluidic polyplexes had a significantly lower PDI value compared to polyplexes prepared by standard pipetting ($p < 0.0001$). These findings highlight the capability of microfluidics to produce monodisperse nanoparticles. Furthermore, the consistent physicochemical characteristics of microfluidic polyplexes at the examined N/P ratios confirm the reproducibility of this method compared to conventional pipetting, with the latter mainly depending on the operator. Both microfluidic preparation and the standard pipetting method produced uniform polyplexes at all examined N/P ratios, highlighting the ability of P(DMAEMA-co-SMA) copolymer to effectively condense DNA (Fig. S2).

Overall, these findings demonstrate the advantages of microfluidics over the conventional pipetting method for the preparation of P(DMAEMA-co-SMA)/DNA polyplexes. Microfluidic development exhibits precise control of size and size distribution with reproducible results. However, the prepared polyplexes exhibited a tendency to aggregate over time, indicating the need for an additional stabilization strategy to improve long-term stability and cellular uptake.

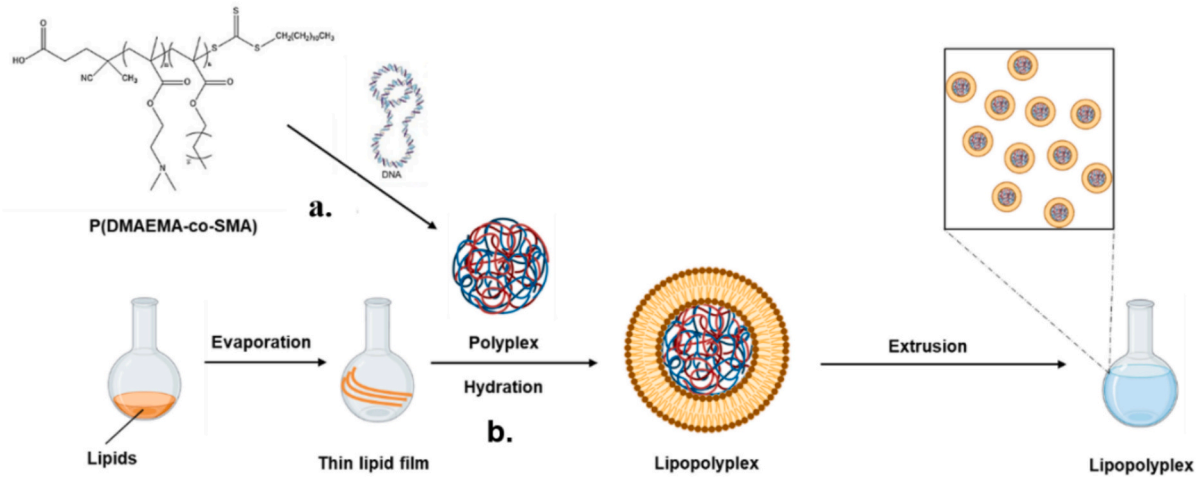

Fig. 4. Preparation of P(DMAEMA-co-SMA)/DNA lipopolyplexes via a two-step process: (a) polyplex formation, and (b) lipid coating of preformed P(DMAEMA-co-SMA)/DNA polyplexes using the thin film hydration/extrusion method. Created with BioRender (https://www.biorender.com/).

Table 2
Physicochemical characteristics of lipopolyplexes.

	D_h (nm)	PDI	ζ-potential (mV)	Encapsulation efficiency (%)
Before Dialysis	182.3 ± 1.0	0.101 ± 0.03	–	–
After Dialysis	250.7 ± 5.2	0.141 ± 0.02	27.5 ± 4.8	67 ± 4

3.4. Development, physicochemical, and morphological characterization of P(DMAEMA-co-SMA)/DNA lipopolyplexes

P(DMAEMA-co-SMA)/DNA lipopolyplexes were developed via a two-step process, in which microfluidic polyplexes at N/P 4 exhibiting the lowest hydrodynamic diameter were used to hydrate a lipid film composed of DSPC:DOPE:Cholesterol:Sphingomyelin:DOTAP (45:35:10:7:3 molar ratio) (Fig. 4). This strategy was utilized to enhance physical stability and retain the advantages of microfluidic preparation. Several studies have demonstrated that lipid coating of polyplexes improves nanoparticle stability, biocompatibility, and transfection efficiency [10,52,53]. Notably, a recent study by Fan et al., reported a similar two-step microfluidics-based approach for lipopolyplex mRNA vaccines, which induced robust immune responses and tumor suppression in both preclinical models and cancer patients [54]. These findings highlight the translational potential of the two-step strategy and demonstrate its relevance for nucleic acid delivery.

In the present study, a biomimetic, membrane-mimicking lipid mixture was used based on mammalian plasma-membrane lipidomics, incorporating the major lipid classes that govern membrane stability, fluidity, and biological interactions [55–57]. Specifically, 45 mol% of the saturated DSPC was incorporated as a helper lipid to enhance the stability of the lipid coating and reduce DNA leakage during prolonged storage, due to its high transition temperature (T_m = 55 °C). Notably, studies have shown that lipid nanoparticles containing 40 mol% DSPC exhibit higher transfection efficiency in vitro compared to nanosystems with lower DSPC content [58]. DOPE was incorporated at 35 mol% due to its established role in promoting endosomal escape through the inverted hexagonal (H_{II}) phase, thus enhancing intracellular gene delivery. DOPE and cholesterol are known to induce the inverted hexagonal (H_{II}) phase in lipid mixtures containing cationic lipids such as DOTAP [59]. Accordingly, cholesterol (10 mol%) and sphingomyelin (7 mol%) were included to reinforce membrane rigidity and promote lipid raft formation, while DOTAP (3 mol%) was added to enhance electrostatic interactions with the preformed polyplexes and facilitate cellular uptake. Polyplexes developed at N/P 4 were selected due to the efficient DNA condensation, favorable physicochemical properties, and minimal copolymer excess, which can contribute to reduced cytotoxicity.

Following lipid coating of the preformed polyplexes, the reduction of positive charge of the lipopolyplexes was achieved by adjusting the pH to 7.4, where P(DMAEMA-co-SMA) is partially protonated. In this way, the external pH was neutralized, and the unbound DNA was removed [60]. As shown in Table 2, lipopolyplexes exhibited a higher mean hydrodynamic diameter after dialysis, and a positive ζ-potential, which is a favorable characteristic for efficient gene delivery. The relatively high encapsulation efficiency demonstrates the effectiveness of this two-step process. Ko et al. reported that a similar procedure with oligonucleotide precondensation using PEI resulted in high encapsulation efficiency, while the same procedure without precondensation resulted in lower encapsulation efficiency [30].

To the best of our knowledge, this is the first report on the development of lipopolyplexes using the amphiphilic pH-responsive cationic copolymer P(DMAEMA-co-SMA) through a two-step process, in which polyplexes were first formed via a 3D-printed microfluidic chip and subsequently coated with lipids in a post-processing step.

The physical stability of lipopolyplexes was evaluated over 84 days,

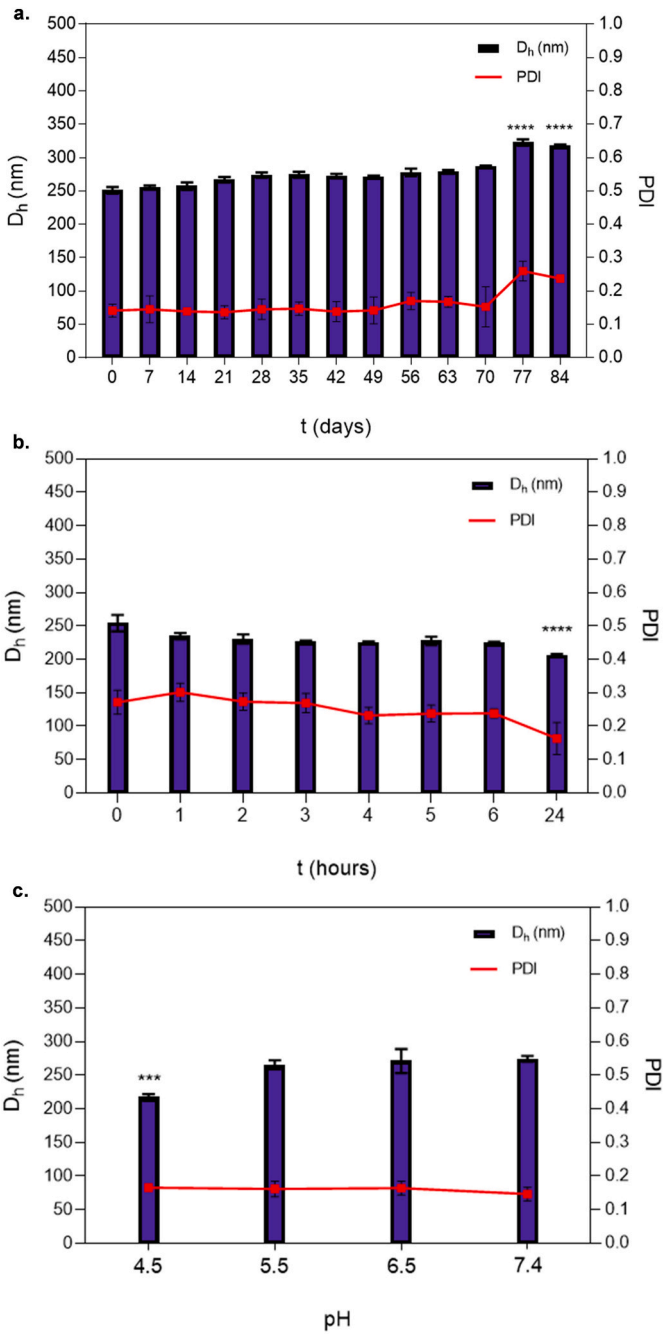

Fig. 5. The hydrodynamic diameter and polydispersity index of lipopolyplexes (a) during prolonged storage, (b) after incubation in complete cell culture medium, and (c) under simulated intracellular pH conditions. Statistical analysis was performed using one-way ANOVA followed by Tukey's post hoc test. Significant differences are denoted relative to the initial formulation at pH 7.4 on the day of preparation (****$p < 0.0001$; ***$p < 0.001$).

as shown in Fig. 5a. The hydrodynamic diameter remained stable at approximately 250 nm for 70 days, after which a significant increase was observed ($p < 0.0001$). During this period, the PDI remained relatively stable and approximately equal to 0.200, indicating that the nanoparticles were considerably uniform with minimal aggregation. The physicochemical properties of the ternary nanocomplexes were also determined in cell culture medium to monitor their behavior under conditions similar to cell assays and to correlate with biological results, such as cytotoxicity [61]. Specifically, interactions with cell culture medium components can affect nanoparticle size, charge, and stability,

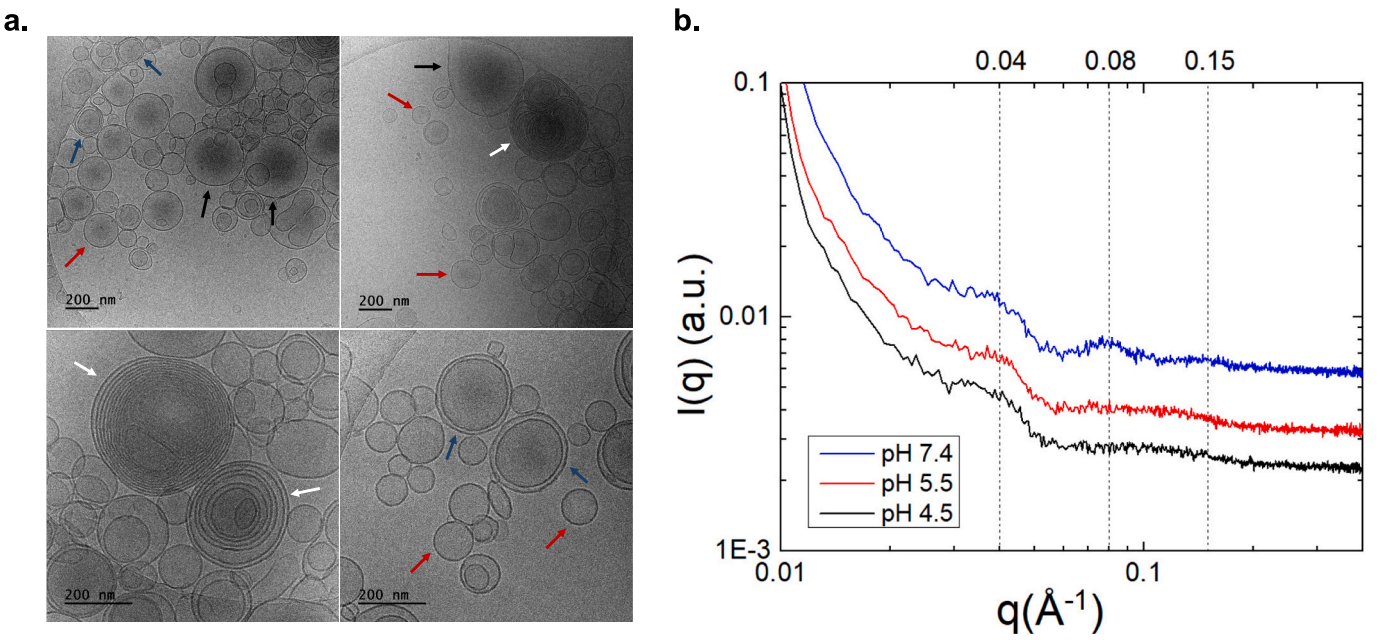

Fig. 6. (a) Cryo-TEM images of the developed lipopolyplexes where multiple coexisting nanostructures can be observed, like vesicles (red arrows), multilamellar vesicles (blue arrows), amorphous particles (black arrows), and classic onion-like lipoplexes (white arrows), and (b) SAXS patterns of lipopolyplexes obtained at pH 4.5, 5.5, and 7.4.

and further influence their in vitro behavior [62]. As shown in Fig. 5b, lipopolyplexes exhibited a slight decrease in size and size distribution, indicating that interactions with cell culture components did not induce aggregation or broadening of the particle population. These findings suggest that the nanocomplexes undergo minor lipid or interfacial rearrangements under biologically relevant conditions, allowing a more direct correlation between physicochemical properties and biological results. Furthermore, incubation of lipopolyplexes at different pH values, mimicking intracellular conditions (early and late endosomes, lysosomes), revealed a significant decrease ($p < 0.001$) in the hydrodynamic diameter at pH 4.5, as measured by dynamic light scattering at 37 °C. This size reduction can be attributed to the increased protonation of the pH-responsive cationic copolymer at lower pH, which enhances electrostatic interactions with DNA and results in a more compact polyplex core (Fig. 5c). These results, combined with the determined buffering capacity of the copolymer, suggest that the lipopolyplexes can maintain their stability in various cellular environments, indicating their potential for effective intracellular gene delivery.

The morphology of the developed lipopolyplexes was determined using cryogenic transmission electron microscopy (cryo-TEM). As shown in Fig. 6a, lipopolyplexes exhibited nanoscale structural heterogeneity, with multiple coexisting nanostructures observed, including vesicles (red arrows), multilamellar vesicles (blue arrows), amorphous particles (black arrows), and classic onion-like lipoplexes (white arrows). These findings suggest that, beyond lipopolyplexes (blue arrows), several competing nanostructures can be formed, including cationic lipid−DNA complexes, and positively charged polyplexes. The multilamellar vesicles, with their concentric layers, indicate the condensation of lipid bilayers with the amorphous P(DMAEMA-co-SMA)/DNA layer attached. The onion-like structures, resembling the classic "sandwich" structure commonly observed in cationic lipid-DNA nanosystems, suggest the proposed mechanism, in which oppositely charged biomolecules act as bridges, stabilizing the nanoparticles [63,64]. In some cases, amorphous particles (black arrows) are also observed, which can be attributed to the prior complexation of the cationic copolymer with DNA [65]. These particles appear optically dense, with thicker lamellar regions compared to the typical onion-like complexes, which are associated with lipoplexes [5,60,66]. The cryo-TEM images reveal morphological diversity with variations in internal nanoscale organization, including interlamellar spacing and internal density, highlighting the structural heterogeneity of the lipopolyplexes. This structural heterogeneity has been widely reported for lipid-polymer hybrid nanosystems and reflects their dynamic self-assembly behavior. Notably, the cryo-TEM images are in accordance with results obtained by Gabelman, indicating that P(DMAEMA-co-SMA)-based lipopolyplexes exhibit structural complexity potentially with both surface- and core-loading [11]. In addition, size distribution analysis obtained from cryo-TEM reveals the presence of a predominant population of lipopolyplexes with diameters of approximately 200 nm (Fig. S3). These findings, along with the stability and encapsulation efficiency results, further indicate the potential of P(DMAEMA-co-SMA)-based lipopolyplexes for efficient nucleic acid delivery.

Small-angle X-ray scattering (SAXS) measurements were also performed to investigate the structural organization of lipopolyplexes under various pH conditions (Fig. 6b). The SAXS patterns at pH 7.4, 5.5, and 4.5 exhibit broad scattering peaks at q values of approximately 0.04, 0.08, and 0.15 $Å^{-1}$, respectively, indicating short-range order. Similar broad reflections at comparable q-values have been reported for lipid-polymer hybrid nanosystems encapsulating siRNA, where combined SAXS and cryo-TEM analyses were interpreted as evidence of a core–shell structure composed of a polymeric core surrounded by concentric lipid bilayers [67]. In this study, the low-q peak of 0.08 $Å^{-1}$ observed at pH 7.4 is consistent with the presence of weakly ordered multilamellar and onion-like nanostructures as revealed by cryo-TEM. Although onion-like vesicles are morphologically well-ordered, the variable interlamellar spacing and structural polydispersity result in broadened SAXS peaks, reflecting limited long-range order. The spacing distance (d-spacing) between the repeating lipid bilayers, calculated from the reflection at a q-value of 0.08 $Å^{-1}$ using the equation $d = 2\pi/q$, is estimated to be 7.85 nm. As pH decreases to 5.5 and 4.5, the scattering peaks at 0.08, and 0.15 $Å^{-1}$ become less pronounced, as shown by the reduced intensity and increased width, suggesting a loss of lamellar organization and/or increased structural disorder under acidic conditions. Despite the lack of a direct correlation between packing density and biological activity, structural information obtained from SAXS can provide valuable insights into the behavior of lipopolyplexes under

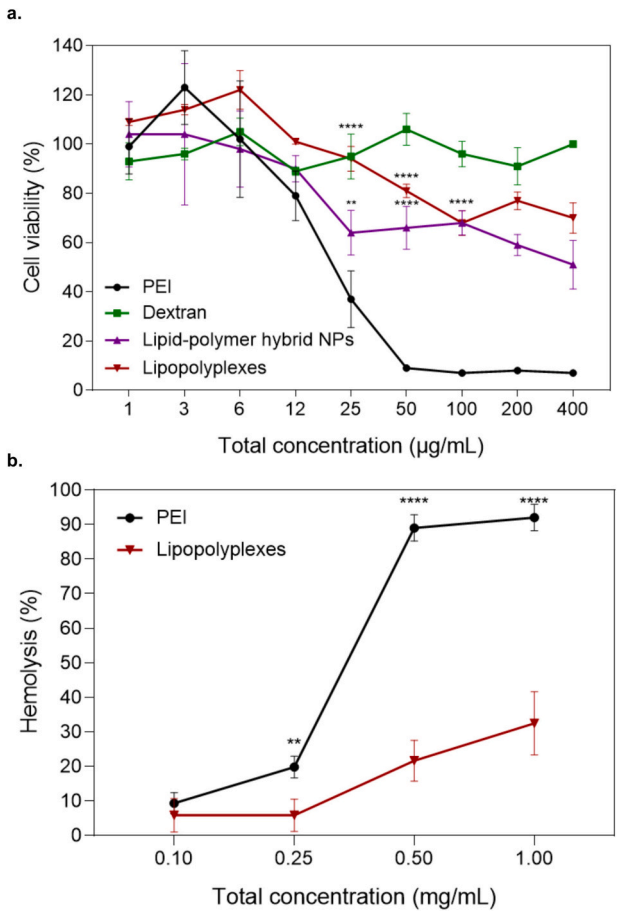

Fig. 7. (a) Cytotoxicity of lipid-polymer hybrid nanoparticles, and lipopolyplexes in HeLa cells after 24 h treatment, with PEI and dextran used as controls, and (b) hemolytic activity induced by P(DMAEMA-co-SMA)-based lipopolyplexes and PEI in RBCs isolated from mice. Statistical significance was determined using two-way ANOVA followed by Bonferroni post-hoc test. Significant differences relative to PEI are denoted (**$p < 0.01$; ****$p < 0.0001$).

biorelevant conditions and their potential structural transitions. This knowledge can contribute to the rational design of such nanosystems with optimized structural stability and controlled nucleic acid release in intracellular environments [68].

3.5. *In vitro cytotoxicity of lipopolyplexes*

The MTT assay was used to evaluate cytotoxicity of the empty nanocarriers (lipid-polymer hybrid nanoparticles) and lipopolyplexes. Studies have shown that cationic nanocarriers enhance transfection efficiency, however, they often induce cytotoxicity due to cell membrane disruption. As shown in Fig. 7a, after 24 h of treatment, both empty nanocarriers and lipopolyplexes composed of P(DMAEMA-co-SMA) exhibit lower cytotoxicity compared to PEI, which is the gold standard in non-viral gene delivery. Specifically, at 50 μg/mL, PEI exhibited a cell viability below 20%, while lipopolyplexes maintained approximately 80% cell viability at the same total concentration. These findings indicate a more biocompatible profile for P(DMAEMA-co-SMA)-based lipopolyplexes within the tested concentration range. It should be noted that this comparison is based on the total formulation concentration and reflects the overall cytotoxicity of the lipid-polymer hybrid nanosystem, rather than the intrinsic cytotoxicity of the copolymer alone. Previous studies have shown that the cytotoxicity of cationic polymers such as PDMAEMA is influenced by their molar mass and N/P ratio [69]. In this study, the amphiphilic statistical copolymer P(DMAEMA-co-SMA) was synthesized with an overall molar mass of 53,900 and an overall DMAEMA segment mass of 42,660 calculated based on copolymer composition. Truong et al., demonstrated that PDMAEMA polymers exhibit minimal cytotoxicity at lower N/P ratios, while higher ratios increase cytotoxicity due to greater charge density and membrane disruption [70]. These findings are in accordance with the lower cytotoxicity observed in HeLa cells for lipopolyplexes compared to PEI. Overall, the results demonstrate that the developed lipid-polymer hybrid nanoparticles and lipopolyplexes are well tolerated within the examined concentration range, with cell viability approximately 70% at 400 μg/mL, which makes them a promising alternative to PEI in non-viral gene delivery. When the treatment duration was extended to 72 h, cell viability remained above 60% within the same concentration range of lipopolyplexes, providing a more comprehensive evaluation of the cytotoxicity (Fig. S4).

In this study, the prepared lipopolyplexes were also assessed regarding their hemolytic activity on fresh RBCs isolated from mice. The hemolytic activity of nanoparticles is a critical parameter that can influence their biocompatibility and clinical application. High hemolytic activity indicates potential damage to red blood cells (RBCs), leading to side effects such as anemia or immune responses. The exact mechanism

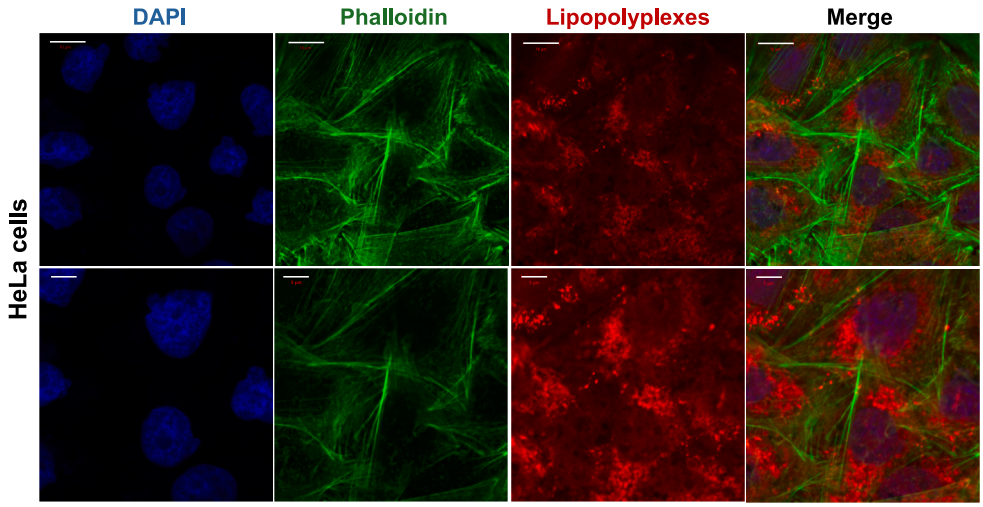

Fig. 8. Confocal laser scanning microscopy (CLSM) images of HeLa cells stained with DAPI (blue) and phalloidin (green) after 24 h of treatment with rhodamine-labelled lipopolyplexes (red) at a concentration of 50 μg/mL. The upper panels show cells at lower magnification (scale bar = 10 μm), while the lower panels correspond to higher magnification images of the same field of view (scale bar = 5 μm).

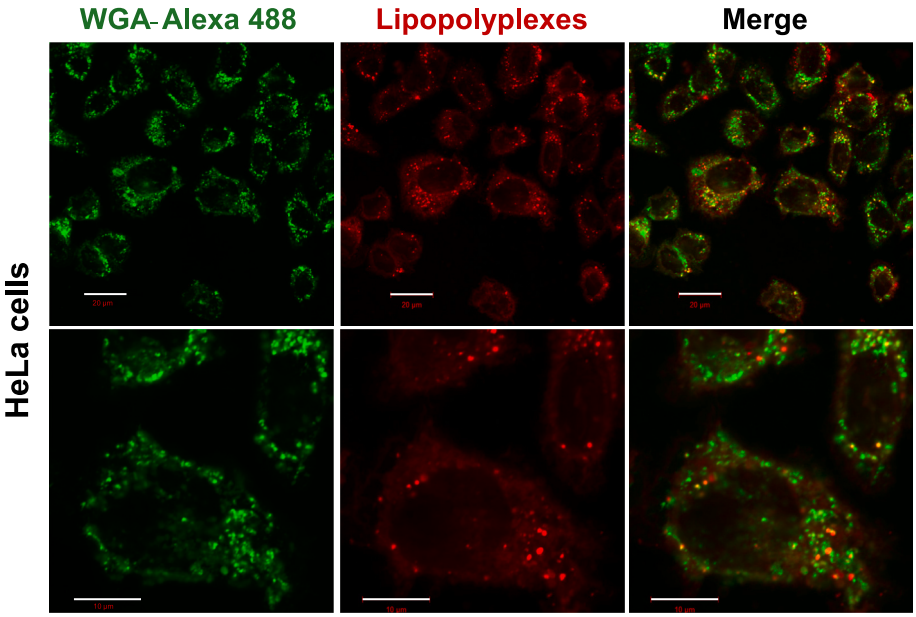

Fig. 9. Confocal laser scanning microscopy (CLSM) images of HeLa cells stained with wheat germ agglutinin (WGA)–Alexa Fluor®488 conjugate (green) after 24 h of treatment with rhodamine-labelled lipopolyplexes (red) at a concentration of 50 μg/mL. The upper panels show cells at lower magnification (scale bar = 20 μm), while the lower panels correspond to higher magnification images of the same field of view (scale bar = 10 μm).

of hemolysis induced by nanoparticles has not been fully elucidated, however it is considered that interactions between RBCs and nanoparticles modulate the level of hemolysis [71]. As shown in Fig. 7b, the prepared lipopolyplexes exhibited low hemolytic activity (<20%) at concentrations up to 0.5 mg/mL, while at 1 mg/mL hemolysis increased to approximately 30%. This increase can be attributed to greater interactions between the positively charged lipopolyplexes and the RBC membrane since it has been reported that hemolytic activity correlates with nanoparticle surface charge [72]. Nevertheless, hemolysis remained lower for lipopolyplexes compared to PEI, which caused consistently higher rates, reaching 90% at concentration 1 mg/mL. These findings demonstrate the potential of P(DMAEMA-co-SMA)-based lipopolyplexes prepared by a two-step microfluidic assisted approach, as a safer and more biocompatible alternative to polycations such as PEI for gene delivery.

3.6. In vitro cellular uptake and distribution of lipopolyplexes

Cellular uptake of lipopolyplexes was assessed by confocal laser scanning microscopy (CLSM) using DAPI to stain nuclei and phalloidin for F-actin visualization. As shown in Fig. 8, rhodamine-labelled lipopolyplexes exhibited a strong internalization signal. This spatial distribution confirms successful cellular uptake and supports the cytoplasmic localization of the lipopolyplexes. Notably, the F-actin architecture remained intact at the tested concentration (50 μg/mL), indicating that cellular uptake of lipopolyplexes occurs without cytotoxic effects on cytoskeletal organization. This finding is particularly significant, as it demonstrates that high nanoparticle internalization can be achieved without compromising cell viability or morphology, which is an essential requirement for the delivery of therapeutic oligonucleotides. Overall, these results, combined with the determined physicochemical properties of the lipopolyplexes, demonstrate that lipid coating can enhance colloidal stability and cellular uptake, while maintaining cytoskeletal integrity.

To further investigate the intracellular trafficking of lipopolyplexes, HeLa cells were incubated for 4 h with WGA-Alexa 488, a lectin that binds plasma membrane glycoproteins and is internalized into endocytic compartments (endosomes and lysosomes) (Fig. 9). Specifically, rhodamine-labelled lipopolyplexes were observed within WGA-positive endocytic vesicles, confirming uptake via endocytosis. Notably, lipopolyplexes were also observed outside the endocytic compartments, indicating successful release into the cytoplasm. This finding demonstrates that the prepared lipopolyplexes are capable of endosomal escape, which is a critical step for efficient intracellular gene delivery that often limits the performance of other nanosystems. It has been reported that cationic lipids, such as DOTAP, which exhibits a permanently charged quaternary ammonium head group, facilitate electrostatic interactions with negatively charged nucleic acids and promote endosomal escape through membrane destabilization. This mechanism protects nucleic acids from degradation before reaching the intracellular site of action [73]. These results demonstrate that the biomimetic lipid coating not only stabilizes the preformed polyplexes but also modulates the biological interactions, including their cytotoxicity, hemocompatibility, and subsequent cellular uptake and intracellular distribution.

4. Conclusion

In this study, a two-step microfluidic approach was utilized to prepare lipid-coated polyplexes using the amphiphilic pH-responsive cationic copolymer P(DMAEMA-co-SMA), DNA 50 bp, and a biomimetic lipid coating. Microfluidic assembly enabled controlled polyplex formation with improved physicochemical properties compared to conventional preparation. Subsequent biomimetic lipid coating of the microfluidic-assembled polyplexes yielded lipopolyplexes with favorable physicochemical properties for gene delivery and enhanced colloidal stability under storage and physiologically relevant conditions. Cryo-TEM analysis revealed the coexistence of multiple nanostructures supported by SAXS data, while in vitro assays confirmed low hemolytic activity, minimal cytotoxicity, and efficient cellular uptake with cytoplasmic distribution, highlighting the favorable biological interactions imparted by the lipid coating. Overall, these findings demonstrate that microfluidic assembly of polyplexes followed by biomimetic lipid coating presents a promising strategy for the preparation of gene delivery nanosystems with improved colloidal stability, biocompatibility and cellular uptake.

Abbreviations

P(DMAEMA-co-SMA)	poly(2-(dimethyl amino ethyl methacrylate)-*co*-(stearyl methacrylate))
PEI	polyethyleneimine
DSPC	1,2-distearoyl-sn-glycero-3-phosphocholine
DOPE	1,2-dioleoyl-sn-glycero-3-phosphoethanolamine
DOTAP	1,2-dioleoyl-3-trimethylammonium-propane
SM	sphingomyelin
DLP 3D printing technology	Digital Light Processing 3D printing technology
SEM	scanning electron microscopy
CLSM	Confocal laser scanning microscopy
DLS	dynamic light scattering
ELS	electrophoretic lights scattering
Cryo-TEM	Cryogenic transmission electron microscopy
SAXS	small angle X-ray scattering

CRediT authorship contribution statement

Ioannis Tsichlis: Writing – original draft, Methodology, Investigation, Formal analysis, Data curation, Conceptualization. **Antiopi Vardaxi:** Methodology, Investigation, Data curation. **Timothy Gomez:** Methodology, Investigation. **Antonia Athanasaki:** Methodology, Investigation. **Alexander Forys:** Methodology, Investigation. **Barbara Trzebicka:** Writing – review & editing, Formal analysis. **Simon C.W. Richardson:** Writing – review & editing, Validation, Data curation. **Kiriaki Chrissopoulou:** Writing – review & editing, Validation, Formal analysis. **Spiros H. Anastasiadis:** Writing – review & editing, Validation, Formal analysis. **Stergios Pispas:** Writing – review & editing, Supervision. **Dennis Douroumis:** Writing – review & editing, Validation, Formal analysis. **Costas Demetzos:** Writing – review & editing, Supervision, Resources, Project administration.

Declaration of competing interest

The authors declare no competing financial interests or personal relationships that could have appeared to influence the work reported in this paper.

Acknowledgements

I.T. acknowledges support from the State Scholarships Foundation (IKY), the British Embassy Athens, and the British Council Greece under the 2nd Call for Greek-British Cooperation on Short-Term PhD Scholarships (Fellowship No. 45657663). The authors thank Professor Michail Rallis for providing mouse red blood cells. The acquisition of the Zetasizer ZSU3105 (Malvern, UK) was supported by Uni-Pharma Kleon Tsetis Pharmaceutical Laboratories S.A. The SAXS measurements were performed on a (GI-)SAXS/WAXS/USAXS instrument, the acquisition of which was supported by the Hellenic Foundation for Research and Innovation (Project SAXS-SOFT, Project Number: 3401). A.A., K.C. and S.H.A. acknowledge partial support by the SAXS-SOFT project.

Appendix A. Supplementary data

Supplementary data to this article can be found online at https://doi.org/10.1016/j.ijbiomac.2026.150678.

Data availability

Data will be made available on request.

References

[1] A. Piperno, M.T. Sciortino, E. Giusto, M. Montesi, S. Panseri, A. Scala, Recent advances and challenges in gene delivery mediated by polyester-based nanoparticles, Int. J. Nanomedicine 16 (2021) 5981–6002, https://doi.org/10.2147/IJN.S321329.
[2] B. Ma, S. Zhang, H. Jiang, B. Zhao, H. Lv, Lipoplex morphologies and their influences on transfection efficiency in gene delivery, J. Control. Release 123 (2007) 184–194, https://doi.org/10.1016/j.jconrel.2007.08.022.
[3] T. Yang, J. Ge, L. Huang, X. Zhu, D. Zhang, S. Tang, J. Zhao, Y. Ma, M. Long, X. Bo, J. Li, Y. Zhang, Q. Yuan, A.D. Sharma, M. Ott, H. Geng, Y. Zhao, L. Zhang, H. Shen, H. Li, D. Li, P. Wan, Q. Xia, Preclinical evaluation of AGT mRNA replacement therapy for primary hyperoxaluria type I disease, Sci. Adv. 11 (2025) eadt9694, https://doi.org/10.1126/sciadv.adt9694.
[4] M. Rezaee, R.K. Oskuee, H. Nassirli, B. Malaekeh-Nikouei, Progress in the development of lipopolyplexes as efficient non-viral gene delivery systems, J. Control. Release 236 (2016) 1–14, https://doi.org/10.1016/j.jconrel.2016.06.023.
[5] A. Ewe, A. Schaper, S. Barnert, R. Schubert, A. Temme, U. Bakowsky, A. Aigner, Storage stability of optimal liposome–polyethylenimine complexes (lipopolyplexes) for DNA or siRNA delivery, Acta Biomater. 10 (2014) 2663–2673, https://doi.org/10.1016/j.actbio.2014.02.037.
[6] Y. Li, T. Yu, L. Han, L. Jin, Y. Jin, J. Quan, Development of a non-viral gene vector for enhancing gene transfection efficiency, J. Drug Delivery Sci. Technol. 75 (2022) 103669, https://doi.org/10.1016/j.jddst.2022.103669.
[7] D. Jiang, A.K. Salem, Optimized dextran-polyethylenimine conjugates are efficient non-viral vectors with reduced cytotoxicity when used in serum containing environments, Int. J. Pharm. 427 (2012) 71–79, https://doi.org/10.1016/j.ijpharm.2011.10.032.
[8] S. Agarwal, Y. Zhang, S. Maji, A. Greiner, PDMAEMA based gene delivery materials, Mater. Today 15 (2012) 388–393, https://doi.org/10.1016/S1369-7021(12)70165-7.
[9] H. Song, G. Wang, B. He, L. Li, C. Li, Y. Lai, X. Xu, Z. Gu, Cationic lipid-coated PEI/DNA polyplexes with improved efficiency and reduced cytotoxicity for gene delivery into mesenchymal stem cells, Int. J. Nanomedicine 7 (2012) 4637–4648, https://doi.org/10.2147/IJN.S33923.
[10] A. Ewe, A. Aigner, Cationic lipid-coated polyplexes (lipopolyplexes) for DNA and small RNA delivery, in: G. Candiani (Ed.), Non-Viral Gene Delivery Vectors: Methods and Protocols, Springer, New York, NY, 2016, pp. 187–200, https://doi.org/10.1007/978-1-4939-3718-9_12.
[11] A. Gabelmann, E. Mansouri-Ghahnavieh, M. Koch, P. Shinde, C.A. Guzmán, B. Loretz, C.-M. Lehr, A novel lipopolyplex platform for dual mRNA delivery via core- and surface-loading, J. Control. Release 384 (2025) 113875, https://doi.org/10.1016/j.jconrel.2025.113875.
[12] E. Mastrobattista, R.H. Kapel, M.H. Eggenhuisen, P.J. Roholl, D.J. Crommelin, W. E. Hennink, G. Storm, Lipid-coated polyplexes for targeted gene delivery to ovarian carcinoma cells, Cancer Gene Ther. 8 (2001) 405–413, https://doi.org/10.1038/sj.cgt.7700311.
[13] Y. Gu, B.M. Reinhard, Membrane fluidity properties of lipid-coated polylactic acid nanoparticles, Nanoscale 16 (2024) 8533–8545, https://doi.org/10.1039/D3NR06464F.
[14] O. Samsonova, C. Pfeiffer, M. Hellmund, O.M. Merkel, T. Kissel, Low molecular weight pDMAEMA-block-pHEMA block-copolymers synthesized via RAFT-polymerization: potential non-viral gene delivery agents? Polymers 3 (2011) 693–718, https://doi.org/10.3390/polym3020693.
[15] A. Vardaxi, S. Pispas, Random cationic copolymers as nanocarriers for ovalbumin, J. Drug Delivery Sci. Technol. 80 (2023) 104177, https://doi.org/10.1016/j.jddst.2023.104177.
[16] T. Sentoukas, C. Demetzos, S. Pispas, Chimeric liposomes incorporating functional copolymers: preparation and pH/thermo-responsive behaviour in aqueous solutions, J. Liposome Res. 31 (2021) 279–290, https://doi.org/10.1080/08982104.2020.1806873.
[17] P.Y. Teo, C. Yang, J.L. Hedrick, A.C. Engler, D.J. Coady, S. Ghaem-Maghami, A.J. T. George, Y.Y. Yang, Hydrophobic modification of low molecular weight polyethylenimine for improved gene transfection, Biomaterials 34 (2013) 7971–7979, https://doi.org/10.1016/j.biomaterials.2013.07.005.
[18] Z. Liu, Z. Zhang, C. Zhou, Y. Jiao, Hydrophobic modifications of cationic polymers for gene delivery, Prog. Polym. Sci. 35 (2010) 1144–1162, https://doi.org/10.1016/j.progpolymsci.2010.04.007.
[19] P. van de Wetering, J.-Y. Cherng, H. Talsma, D.J.A. Crommelin, W.E. Hennink, 2-(dimethylamino)ethyl methacrylate based (co)polymers as gene transfer agents, J. Control. Release 53 (1998) 145–153, https://doi.org/10.1016/S0168-3659(97)00248-4.
[20] D. Putnam, Polymers for gene delivery across length scales, Nat. Mater. 5 (2006) 439–451, https://doi.org/10.1038/nmat1645.
[21] V. Chrysostomou, H. Katifelis, M. Gazouli, K. Dimas, C. Demetzos, S. Pispas, Hydrophilic random cationic copolymers as polyplex-formation vectors for DNA, Materials 15 (2022) 2650, https://doi.org/10.3390/ma15072650.
[22] Y.-P. Ho, C.L. Grigsby, F. Zhao, K.W. Leong, Tuning physical properties of nanocomplexes through microfluidics-assisted confinement, Nano Lett. 11 (2011) 2178–2182, https://doi.org/10.1021/nl200862n.
[23] A. Agha, W. Waheed, I. Stiharu, V. Nerguizian, G. Destgeer, E. Abu-Nada, A. Alazzam, A review on microfluidic-assisted nanoparticle synthesis, and their applications using multiscale simulation methods, Discov. Nano 18 (2023) 18, https://doi.org/10.1186/s11671-023-03792-x.

[24] S. Gimondi, H. Ferreira, R.L. Reis, N.M. Neves, Microfluidic devices: a tool for nanoparticle synthesis and performance evaluation, ACS Nano 17 (15) (2023) 14205–14228, https://doi.org/10.1021/acsnano.3c01117. Epub 2023 Jul 27. PMID: 37498731; PMCID: PMC10416572.
[25] S.J. Shepherd, D. Issadore, M.J. Mitchell, Microfluidic formulation of nanoparticles for biomedical applications, Biomaterials 274 (2021) 120826, https://doi.org/10.1016/j.biomaterials.2021.120826.
[26] K. Rahali, A.G. Tabriz, D. Douroumis, The effect of 3D printed microfluidic array designs on the preparation of liposome nanoparticles, J. Drug Delivery Sci. Technol. 94 (2024) 105411, https://doi.org/10.1016/j.jddst.2024.105411.
[27] H. Sadeghpour, B. Khalvati, E. Entezar-Almahdi, N. Savadi, S. Hossaini Alhashemi, M. Raoufi, A. Dehshahri, Double domain polyethylenimine-based nanoparticles for integrin receptor mediated delivery of plasmid DNA, Sci. Rep. 8 (2018) 6842, https://doi.org/10.1038/s41598-018-25277-z.
[28] L. Hu, S. Li, Y. Lv, pH-sensitive cationic polymer/DNA nano-assemblies for efficient gene transfection in neuroma cells, ACS Appl. Nano Mater. 6 (2023) 10559–10568, https://doi.org/10.1021/acsanm.3c01520.
[29] D.P. Feldmann, Y. Xie, S.K. Jones, D. Yu, A. Moszczynska, O.M. Merkel, The impact of microfluidic mixing of triblock micelleplexes on in vitro/in vivo gene silencing and intracellular trafficking, Nanotechnology 28 (2017) 224001, https://doi.org/10.1088/1361-6528/aa6d15.
[30] Y.T. Ko, R. Bhattacharya, U. Bickel, Liposome encapsulated polyethylenimine/ODN polyplexes for brain targeting, J. Control. Release 133 (2009) 230–237, https://doi.org/10.1016/j.jconrel.2008.10.013.
[31] R. Pattipeiluhu, Y. Zeng, M.M.R.M. Hendrix, I.K. Voets, A. Kros, T.H. Sharp, Liquid crystalline inverted lipid phases encapsulating siRNA enhance lipid nanoparticle mediated transfection, Nat. Commun. 15 (2024) 1303, https://doi.org/10.1038/s41467-024-45666-5.
[32] I. Tsichlis, A.-P. Manou, V. Manolopoulou, K. Matskou, M. Chountoulesi, V. Pletsa, A. Xenakis, C. Demetzos, Development of liposomal and liquid crystalline lipidic nanoparticles with non-ionic surfactants for quercetin incorporation, Materials 16 (2023) 5509, https://doi.org/10.3390/ma16165509.
[33] E.-M. Kosti, H. Sotiropoulou, I. Tsichlis, M. Tsakiri, N. Naziris, C. Demetzos, Impact of pluronic F-127 on the stability of quercetin-loaded liposomes: insights from DSC preformulation studies, Materials 17 (2024) 5454, https://doi.org/10.3390/ma17225454.
[34] M. Chountoulesi, N. Pippa, V. Chrysostomou, S. Pispas, E.D. Chrysina, A. Forys, L. Otulakowski, B. Trzebicka, C. Demetzos, Stimuli-responsive lyotropic liquid crystalline nanosystems with incorporated poly(2-dimethylamino ethyl methacrylate)-b-poly(lauryl methacrylate) amphiphilic block copolymer, Polymers 11 (2019) 1400, https://doi.org/10.3390/polym11091400.
[35] T.L. Moore, D.A. Urban, L. Rodriguez-Lorenzo, A. Milosevic, F. Crippa, M. Spuch-Calvar, S. Balog, B. Rothen-Rutishauser, M. Lattuada, A. Petri-Fink, Nanoparticle administration method in cell culture alters particle-cell interaction, Sci. Rep. 9 (2019) 900, https://doi.org/10.1038/s41598-018-36954-4.
[36] E. Samaridou, H. Walgrave, E. Salta, D.M. Álvarez, V. Castro-López, M. Loza, M. J. Alonso, Nose-to-brain delivery of enveloped RNA - cell permeating peptide nanocomplexes for the treatment of neurodegenerative diseases, Biomaterials 230 (2020) 119657, https://doi.org/10.1016/j.biomaterials.2019.119657.
[37] L. Cui, S. Renzi, E. Quagliarini, L. Digiacomo, H. Amenitsch, L. Masuelli, R. Bei, G. Ferri, F. Cardarelli, J. Wang, A. Amici, D. Pozzi, C. Marchini, G. Caracciolo, Efficient delivery of DNA using lipid nanoparticles, Pharmaceutics 14 (2022) 1698, https://doi.org/10.3390/pharmaceutics14081698.
[38] N. Naziris, N. Pippa, V. Chrysostomou, S. Pispas, C. Demetzos, M. Libera, B. Trzebicka, Morphological diversity of block copolymer/lipid chimeric nanostructures, J. Nanopart. Res. 19 (2017) 347, https://doi.org/10.1007/s11051-017-4021-5.
[39] Simon C.W. Richardson, Hanno V.J. Kolbe, R. Duncan, Potential of low molecular mass chitosan as a DNA delivery system: biocompatibility, body distribution and ability to complex and protect DNA, Int. J. Pharm. 178 (1999) 231–243, https://doi.org/10.1016/S0378-5173(98)00378-0.
[40] Y. Cheng, C.D. Hay, S.M. Mahuttanatan, J.W. Hindley, O. Ces, Y. Elani, Microfluidic technologies for lipid vesicle generation, Lab Chip 24 (2024) 4679–4716, https://doi.org/10.1039/D4LC00380B.
[41] H. Zhang, J. Yang, R. Sun, S. Han, Z. Yang, L. Teng, Microfluidics for nano-drug delivery systems: from fundamentals to industrialization, Acta Pharm. Sin. B 13 (2023) 3277–3299, https://doi.org/10.1016/j.apsb.2023.01.018.
[42] S.J. Shepherd, C.C. Warzecha, S. Yadavali, R. El-Mayta, M.-G. Alameh, L. Wang, D. Weissman, J.M. Wilson, D. Issadore, M.J. Mitchell, Scalable mRNA and siRNA lipid nanoparticle production using a parallelized microfluidic device, Nano Lett. 21 (2021) 5671–5680, https://doi.org/10.1021/acs.nanolett.1c01353.
[43] S. Yu, J. Chen, R. Dong, Y. Su, B. Ji, Y. Zhou, X. Zhu, D. Yan, Enhanced gene transfection efficiency of PDMAEMA by incorporating hydrophobic hyperbranched polymer cores: effect of degree of branching, Polym. Chem. 3 (2012) 3324–3329, https://doi.org/10.1039/C2PY20487H.
[44] C. Liu, P. Ni, X. Fang, X. Zhou, Synthesis of amphiphilic diblock copolymers poly[2-(N, N-dimethylamino)ethyl methacrylate]-b-poly(stearyl methacrylate) and their self-assembly in mixed solvent, Colloid Polym. Sci. 287 (2009) 45–55, https://doi.org/10.1007/s00396-008-1951-6.
[45] S.A. Chew, M.C. Hacker, A. Saraf, R.M. Raphael, F.K. Kasper, A.G. Mikos, Biodegradable branched polycationic polymers with varying hydrophilic spacers for non-viral gene delivery, Biomacromolecules 10 (2009) 2436–2445, https://doi.org/10.1021/bm9003783.
[46] B. Singh, S. Maharjan, T.-E. Park, T. Jiang, S.-K. Kang, Y.-J. Choi, C.-S. Cho, Tuning the buffering capacity of polyethylenimine with glycerol molecules for efficient gene delivery: staying in or out of the endosomes, Macromol. Biosci. 15 (2015) 622–635, https://doi.org/10.1002/mabi.201400463.
[47] A. Kargaard, J.P.G. Sluijter, B. Klumperman, Polymeric siRNA gene delivery – transfection efficiency versus cytotoxicity, J. Control. Release 316 (2019) 263–291, https://doi.org/10.1016/j.jconrel.2019.10.046.
[48] J.M. Layman, S.M. Ramirez, M.D. Green, T.E. Long, Influence of polycation molecular weight on poly(2-dimethylaminoethyl methacrylate)-mediated DNA delivery in vitro, Biomacromolecules 10 (2009) 1244–1252, https://doi.org/10.1021/bm9000124.
[49] R.A. Jones, M.H. Poniris, M.R. Wilson, pDMAEMA is internalised by endocytosis but does not physically disrupt endosomes, J. Control. Release 96 (2004) 379–391, https://doi.org/10.1016/j.jconrel.2004.02.011.
[50] P. van de Wetering, J.-Y. Cherng, H. Talsma, W.E. Hennink, Relation between transfection efficiency and cytotoxicity of poly(2-(dimethylamino)ethyl methacrylate)/plasmid complexes, J. Control. Release 49 (1997) 59–69, https://doi.org/10.1016/S0168-3659(97)00059-X.
[51] S. Liu, S. Deng, X. Li, D. Cheng, Size- and surface-dual engineered small polyplexes for efficiently targeting delivery of siRNA, Molecules 26 (2021) 3238, https://doi.org/10.3390/molecules26113238.
[52] S. Thalmayr, M. Grau, L. Peng, J. Pöhmerer, U. Wilk, P. Folda, M. Yazdi, E. Weidinger, T. Burghardt, M. Höhn, E. Wagner, S. Berger, Molecular chameleon carriers for nucleic acid delivery: the sweet spot between lipoplexes and polyplexes, Adv. Mater. 35 (2023) 2211105, https://doi.org/10.1002/adma.202211105.
[53] Q.-Y. Zhang, P.Y. Ho, M.-J. Tu, J.L. Jilek, Q.-X. Chen, S. Zeng, A.-M. Yu, Lipidation of polyethylenimine-based polyplex increases serum stability of bioengineered RNAi agents and offers more consistent tumoral gene knockdown in vivo, Int. J. Pharm. 547 (2018) 537–544, https://doi.org/10.1016/j.ijpharm.2018.06.026.
[54] T. Fan, C. Xu, J. Wu, Y. Cai, W. Cao, H. Shen, M. Zhang, H. Zhu, J. Yang, Z. Zhu, X. Ma, J. Ren, L. Huang, Q. Li, Y. Tang, B. Yu, C. Chen, M. Xu, Q. Wang, Z. Xu, F. Chen, S. Liang, Z. Zhong, A. Jamroze, D.G. Tang, H. Li, C. Dong, Lipopolyplex-formulated mRNA cancer vaccine elicits strong neoantigen-specific T cell responses and antitumor activity, Sci. Adv. 10 (2024) eadn9961, https://doi.org/10.1126/sciadv.adn9961.
[55] J. Symons, K.-J. Cho, J. Chang, G. Du, M.N. Waxham, J.F. Hancock, I. Levental, K. R. Levental, Lipidomic atlas of mammalian cell membranes reveals hierarchical variation induced by culture conditions, subcellular membranes, and cell lineages, Soft Matter 17 (2021) 288–297, https://doi.org/10.1039/d0sm00404a.
[56] J.L. Sampaio, M.J. Gerl, C. Klose, C.S. Ejsing, H. Beug, K. Simons, A. Shevchenko, Membrane lipidome of an epithelial cell line, Proc. Natl. Acad. Sci. U. S. A. 108 (2011) 1903–1907, https://doi.org/10.1073/pnas.1019267108.
[57] K.R. Levental, E. Malmberg, J.L. Symons, Y.-Y. Fan, R.S. Chapkin, R. Ernst, I. Levental, Lipidomic and biophysical homeostasis of mammalian membranes counteracts dietary lipid perturbations to maintain cellular fitness, Nat. Commun. 11 (2020) 1339, https://doi.org/10.1038/s41467-020-15203-1.
[58] N. Chander, G. Basha, M.H.Y. Cheng, D. Witzigmann, P.R. Cullis, Lipid nanoparticle mRNA systems containing high levels of sphingomyelin engender higher protein expression in hepatic and extra-hepatic tissues, Mol. Ther. Methods Clin. Develop. 30 (2023) 235–245, https://doi.org/10.1016/j.omtm.2023.06.005.
[59] I.M. Hafez, N. Maurer, P.R. Cullis, On the mechanism whereby cationic lipids promote intracellular delivery of polynucleic acids, Gene Ther. 8 (2001) 1188–1196, https://doi.org/10.1038/sj.gt.3301506.
[60] C.G. Koh, X. Zhang, S. Liu, S. Golan, B. Yu, X. Yang, J. Guan, Y. Jin, Y. Talmon, N. Muthusamy, K.K. Chan, J.C. Byrd, R.J. Lee, G. Marcucci, L.J. Lee, Delivery of antisense oligodeoxyribonucleotide lipopolyplex nanoparticles assembled by microfluidic hydrodynamic focusing, J. Control. Release 141 (2010) 62–69, https://doi.org/10.1016/j.jconrel.2009.08.019.
[61] B. Meesaragandla, Y. Komaragiri, R. Schlüter, O. Otto, M. Delcea, The impact of cell culture media on the interaction of biopolymer-functionalized gold nanoparticles with cells: mechanical and toxicological properties, Sci. Rep. 12 (2022) 16643, https://doi.org/10.1038/s41598-022-20691-w.
[62] T.L. Moore, L. Rodriguez-Lorenzo, V. Hirsch, S. Balog, D. Urban, C. Jud, B. Rothen-Rutishauser, M. Lattuada, A. Petri-Fink, Nanoparticle colloidal stability in cell culture media and impact on cellular interactions, Chem. Soc. Rev. 44 (2015) 6287–6305, https://doi.org/10.1039/C4CS00487F.
[63] J.L. Paris, R. Gaspar, F. Coelho, P.A.A. De Beule, B.F.B. Silva, Stability criterion for the assembly of core–shell lipid–polymer–nucleic acid nanoparticles, ACS Nano 17 (2023) 17587–17594, https://doi.org/10.1021/acsnano.3c07204.
[64] S. Weisman, D. Hirsch-Lerner, Y. Barenholz, Y. Talmon, Nanostructure of cationic lipid-oligonucleotide complexes, Biophys. J. 87 (2004) 609–614, https://doi.org/10.1529/biophysj.103.033480.
[65] X. Yang, C.G. Koh, S. Liu, X. Pan, R. Santhanam, B. Yu, Y. Peng, J. Pang, S. Golan, Y. Talmon, Y. Jin, N. Muthusamy, J.C. Byrd, K.K. Chan, L.J. Lee, G. Marcucci, R. J. Lee, Transferrin receptor-targeted lipid nanoparticles for delivery of an antisense oligodeoxyribonucleotide against Bcl-2, Mol. Pharm. 6 (2009) 221–230, https://doi.org/10.1021/mp800149s.
[66] T. Tagawa, M. Manvell, N. Brown, M. Keller, E. Perouzel, K.D. Murray, R. P. Harbottle, M. Tecle, F. Booy, M.C. Brahimi-Horn, C. Coutelle, N.R. Lemoine, E. W.F.W. Alton, A.D. Miller, Characterisation of LMD virus-like nanoparticles self-assembled from cationic liposomes, adenovirus core peptide μ (mu) and plasmid DNA, Gene Ther. 9 (2002) 564–576, https://doi.org/10.1038/sj.gt.3301686.
[67] A. Aljabbari, A.G. Lokras, J.J.K. Kirkensgaard, T. Rades, H. Franzyk, A. Thakur, Y. Zhang, C. Foged, Elucidating the nanostructure of small interfering RNA-loaded lipidoid-polymer hybrid nanoparticles, J. Colloid Interface Sci. 633 (2023) 907–922, https://doi.org/10.1016/j.jcis.2022.11.141.

[68] C. Wilhelmy, L. Uebbing, B. Kolb, M.A. Graewert, T. Nawroth, H. Haas, P. Langguth, Direct structural investigation of pH responsiveness in mRNA lipid nanoparticles: refining paradigms, J. Control. Release 384 (2025) 113848, https://doi.org/10.1016/j.jconrel.2025.113848.

[69] A. Dinari, T.T. Moghadam, M. Abdollahi, M. Sadeghizadeh, Synthesis and characterization of a nano-polyplex system of GNRs-PDMAEA-pDNA: an inert self-catalyzed degradable carrier for facile gene delivery, Sci. Rep. 8 (2018) 8112, https://doi.org/10.1038/s41598-018-26260-4.

[70] N.P. Truong, Z. Jia, M. Burgess, L. Payne, N.A.J. McMillan, M.J. Monteiro, Self-catalyzed degradable cationic polymer for release of DNA, Biomacromolecules 12 (2011) 3540–3548, https://doi.org/10.1021/bm2007423.

[71] S. Yedgar, G. Barshtein, A. Gural, Hemolytic activity of nanoparticles as a marker of their hemocompatibility, Micromachines (Basel) 13 (2022) 2091, https://doi.org/10.3390/mi13122091.

[72] E. Samaridou, J. Simon, M. Beck-Broichsitter, G. Davidson, P.A. Levkin, Rational design of unsaturated, thioether ionizable lipids for enhanced in vivo mRNA delivery, Adv. Healthc. Mater. 14 (2025) 2501037, https://doi.org/10.1002/adhm.202501037.

[73] E.P. Lamparelli, E. Ciaglia, M.C. Ciardulli, V. Lopardo, F. Montella, A.A. Puca, G. Della Porta, Optimizing mRNA delivery: a microfluidic exploration of DOTMA vs. DOTAP lipid nanoparticles for GFP expression on human PBMCs and THP-1 cell line, Int. J. Pharm. 672 (2025) 125324, https://doi.org/10.1016/j.ijpharm.2025.125324.